"Babeş-Bolyai" University, Faculty of Physics

&

University of Medicine and Pharmacy "Iuliu Haţieganu", Faculty of Pharmacy,

Cluj-Napoca, Romania

NANOSTRUCTURED SYSTEMS WITH POTENTIAL APPLICATIONS AS CONTRAST AGENTS IN MAGNETIC RESONANCE IMAGING AND DRUG CARRIERS

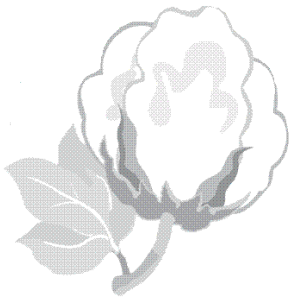

Summary of PhD Thesis

Violeta Corina Moraru (n. Hebrişţean)

Scientific coordinators:

Prof. Dr. Simion SIMON

Prof. Dr. Felicia LOGHIN

Cluj-Napoca, 2015

CONTENTS

KEYWORDS: silica nanostructured particles, liposomes, theranostic, MRI, contrast agents, gadolinium, cancer, gossypol, cotton seeds, drug delivery.

1. INTRODUCTION

In recent decades, nanotechnology has a significant impact on clinical therapeutics. Advances in nanostructured drug carriers such as silica nanoparticles and liposomes have enabled more efficient and safer drug delivery. These advantages include improved pharmacokinetics and reduced side effects. In cancer treatments, because of the leaky tumour vasculatures, nanoparticles can better accumulate at the tumour sites due to the vascular enhanced permeability and retention effect. These benefits have made nanoparticles a promising candidate to replace traditional chemotherapy, with good results in limiting side effects. Nanostructured materials are particularly well suited to theranostic applications (therapy simultaneous with diagnoses) because they can upload contrast agents for traceable imaging and also to carry drug payloads for therapeutic intervention.

This study was conducted in order to apply the new innovations in the field of materials nanotechnology to improve some drug delivery systems release and as well to obtain theranostic systems with the simultaneous ability to treat and to diagnose.

This doctoral thesis is organised in five chapters including the present introduction and general conclusions. Chapter 2 deals with silica materials and liposomes and topics related to their application on drug delivery systems. This chapter continues with presenting aspects regarding the compounds proposed in this thesis to be loaded in the porous silica and liposomes, more specific, *Gossypium hirsutum* (cotton plant) and gadolinium compounds along with their pharmaceutical properties. Chapter 3 presents theoretical aspects of device's operating principles used in this research. Chapter 4 deals with the experimental results and discussion organised in journal articles submitted or ready for submission. It comprises four parts. Subchapter 4.1 discusses loading of cotton seeds extract in silica matrix prepared by sol-gel method, evaluates its new properties and how drying process influences compounds release from the matrix. In Subchapter 4.2 a theranostic pilot system is proposed. Silica-gadolinium particles prepared by sol-gel method are loaded with gossypol, a polyphenolic compound from cotton plant, and their characteristics are evaluated in order to be used as theranostic compounds, with anticancer therapeutic properties from gossypol and with diagnostic properties related to gadolinium as contrast agent in magnetic resonance imaging. In Subchapter 4.3 the proposed system is similar to the one discussed in Subchapter 4.2, but with some advantages: particles are nanosized, highly porous, able to entrap a high quantity of gossypol and with appropriate relaxivity properties. Chapter 4.4 continues with a different system proposed to

encapsulate gadolinium compounds and gossypol: liposomes. Finally, Chapter 5 presents general conclusions summarizing the significance of the research done in this thesis.

2. SYNTHESIS AND CHARACTERISATION OF *GOSSYPIUM HIRSUTUM* SEEDS EXTRACT NANOENCAPSULATED IN SILICA MICROPARTICLES

2.1. Main objectives

The nanoencapsulation of pharmaceutically active natural compounds into porous systems through sol-gel method can lead to new materials with sustained release behaviour of the entrapped pharmaceuticals. This paper reports on the properties of inorganic silica microparticles loaded with cotton (*Gossypium hirsutum)* seeds extract and release characteristics, according to drying methods used in the synthesis: freeze and heat drying. An *in vitro* release study was carried out in release media with pH 1.1 and 7.4, and mathematical models for release kinetics were applied to assess the effects of drying process and pH on the release characteristics. To the best of our knowledge there is no study on *Gossypium hirsutum* cotton seeds extract encapsulated in silica matrices.

2.2. Synthesis and characterization methods

Gossypium hirsutum seeds extract preparation consists in ethanol extraction from cotton seeds in dark conditions for 30 days. *Gossypium hirsutum* seeds extract was loaded into silica matrix by mixing the silica sol prepared by sol-gel method with *Gossypium Hirsutum* alcoholic extract (GH) in 1:2 volumic ratio. Half of the gel obtained after two weeks was dried at 37 °C and thereafter at 110 °C for 1 h. The other half was freeze dried. For comparison, as control, we also synthesised pure silica, and for a correct assessment GH was replaced with the same amount of 70° ethanol. The samples will be further denoted as SiO_2-HD (HD - heat dried) and SiO_2-FD (FD - freeze dried), and the corresponding *Gossypium Hirsutum* seeds extract (GH) loaded silica formulations will be denoted as SiO_2-GH-HD and SiO_2-GH-FD.

Alcoholic extract of *Gossypium hirsutum* seeds was first characterized by High Performance Liquid Chromatography (HPLC) and Fourier Transform Infrared Spectroscopy (FT-IR). The loaded and unloaded silica xerogels obtained after heat or freeze drying were further investigated by FT-IR, X-Ray Diffraction (XRD), Dynamic Light Scattering (DLS), Differential thermal analysis/Thermogravimetric analysis (DTA/TGA), UV-Vis Diffuse Reflectance spectroscopy (UV-Vis DRS) and fluorescence

spectroscopy. The effects of drying process on both silica particles and plant extract were in more detail evaluated by FT-IR spectroscopy.

In vitro release study of plant extract was carried out at 37 °C under rotation conditions at 1.1 and 7.4 pH values. The absorbance of the removed release medium was measured with a UV–Vis spectrophotometer at a wavelength of 280 nm, against an appropriate blank. To determine the amount of extract released from each sample, a standard calibration curve was used.

2.3. Results and discussion

Characterisation of Gossypium hirsutum extract

Using column chromatography, fractionation of phenolic extracts from cotton seeds extract has been possible. The polyphenols eluted in less than 35 minutes are summarized in Table 1.

According to the literature, the polyphenols identified in leaves of cotton plant are gallic, caffeic, syringic, chlorogenic, ferulic, vanillic, cinnamic, p-coumaric, salicylic, galfic, gentisic, protocatechuic, benzoic, p-hydroxybenzoic and sinapic acids along with catechin and flavonoids (isoquercitrin glycoside, rutin and kaempferol-3-rutinoside) [1-3]. In our cotton seeds extract we identified caftaric, gentisic, caffeic, chlorogenic, p-coumaric and ferulic acid along with flavonoids (isoquercitrin, rutoside and quercetol) which was the predominant group, with rutoside (peak no. 3) the major component from the polyphenols identified (Figure 1 and Table 1).

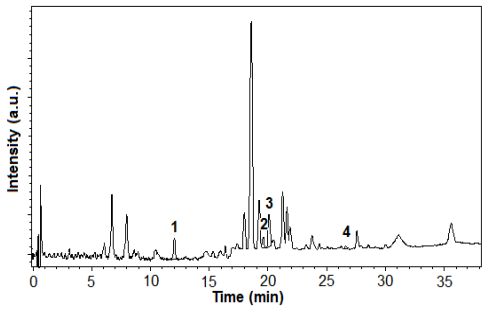

Figure 1. HPLC chromatogram of polyphenols in cotton seeds extract

Table 1. HPLC main peaks (polyphenols in cotton seeds extract)

No.	Compound	Conc. (µg/ml)
	Caftaric acid	-
	Gentisic acid	-
	Caffeic acid	-
	Chlorogenic acid	-
	p-coumaric acid	-
1	Ferulic acid	0.810
2	Isoquercitrin	1.152
3	Rutoside	3.529
4	Quercetol	0.179

The FT-IR spectrum of nonentrapped GH (Figure 2) shows vibrational bands that can be grouped more or less according to their corresponding compounds (Table 2) [4-7].

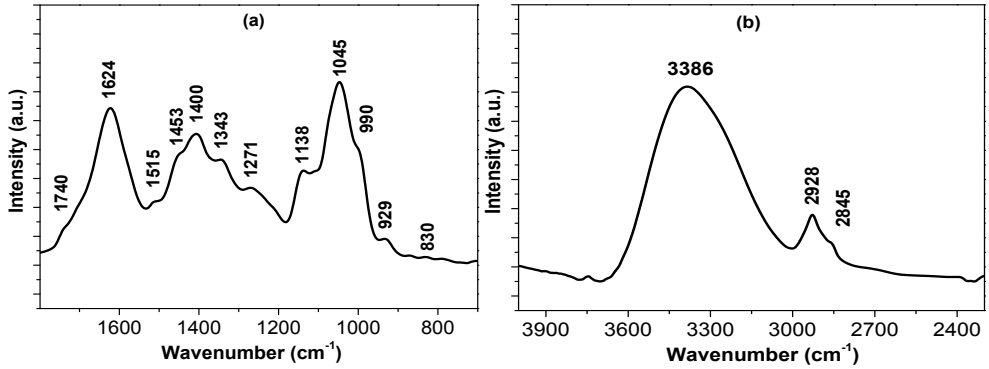

Figure 2. FT-IR spectrum of nonentrapped GH in (a) 700-1800 cm^{-1} and (b) 2300-4000 cm^{-1} ranges

Table 2. Assignment of FT-IR absorption bands

Wavenumber (cm^{-1})	Vibration type	Compounds
<1000 cm^{-1}	C-H bending	isoprenoids
997-1130 cm^{-1}	C-O stretching	mono-,oligo- and carbohydrates
1045 cm^{-1}		cellulose and hemicellulose
1150-1270 cm^{-1}	carbonyl C-O stretching O-H bending	
1300-1450 cm^{-1}	C-O stretching C-C stretching	amide phenyl groups
1500-1600 cm^{-1}	aromatic domain N-H bending	aromatic compounds amines
1600-1760 cm^{-1}	N-H bending C=O stretching	amino acids aldehydes, ketones, esters
1740 cm^{-1}	C=C stretching	total phenols
2800-2930 cm^{-1}	C-H stretching (CH_3 and CH_2) C-H including *cis* double bonds	methoxy derivatives from aldehydes, lipids
3350-3600 cm^{-1}	OH stretching	water, alcohols, phenols, carbohydrates, peroxides, proteins,
3413 cm^{-1}		fatty acids, lignin cellulose and
3650 cm^{-1}	NH stretching	hemicellulose amides

All these specific bands indicate the presence of amino acids, carbohydrates, amides, amines, aldehydes, ketones, esters, glycerides, alcohols, phenols, isoprenoids and other compounds that have in structure the identified functional groups.

Because the drying method could cause changes in chemical structure of the pharmaceutically active compounds from cotton seeds extract, it was considered necessary to investigate this by FT-IR spectroscopy.

The absorbance band for freeze dried samples at around 1624 cm^{-1} (C=O and C=C stretching vibrations) decreases, suggesting that ketone groups and unsaturated double bonds react chemically. B-ring from flavonoids may have been modified because no specific band is observed at around 1557 cm^{-1}. The decrease of the peak at 1343 cm^{-1} in the freeze dried GH spectra also indicates the reaction of flavonoids adjacent dihydroxyl groups from B-ring [8] (Figure 3a).

The absorbance band around 1045 cm^{-1} recorded from 37°C dried sample is shifted in heat dried GH towards higher values (around 1085 cm^{-1}). This band is characteristic to C-O stretching in mono-oligo- and carbohydrates and proves changing in carbohydrate chemical composition. The intensity of the bands occurring between 700 and 950 cm^{-1} increases too, denoting changing in isoprenoids chemical structure.

The FT-IR spectra of both heat dried and freeze dried GH show changes also in the broad band from around 3400 cm^{-1} (Figure 3b) corresponding to the O-H stretching vibration in alcohols (3600-3300 cm^{-1}) and carboxylic acids (3300-2500 cm^{-1}) present in carbohydrates. The shoulder that appears at around 3200 cm^{-1} in the spectrum of heat dried GH might denote the increase in carboxylic acids due to primary OH oxidation and/or hydrolysis of acetyl groups from carbohydrates.

All these effects related to the drying conditions of the investigated compounds may influence the GH composition, and it is difficult to assume how their therapeutic properties might be affected.

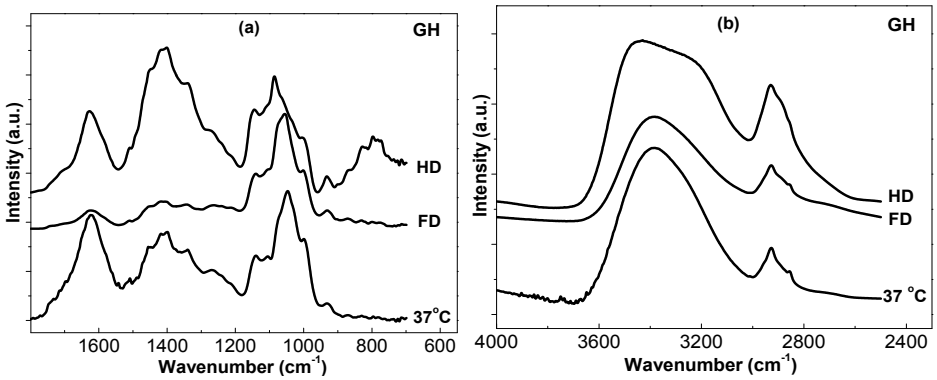

Figure 3. FT-IR spectra of nonentrapped GH heat dried (HD), freeze dried (FD) and 37 °C dried in (a) 700-1800 cm^{-1} and (b) 2500-4000 cm^{-1} ranges

Characterisation of Gossypium hirsutum loaded silica

The XRD patterns of silica samples (Figure 4) indicate the amorphous state, even after GH loading, amorphous silica particles being considered less toxic than crystalline particles [9, 10].

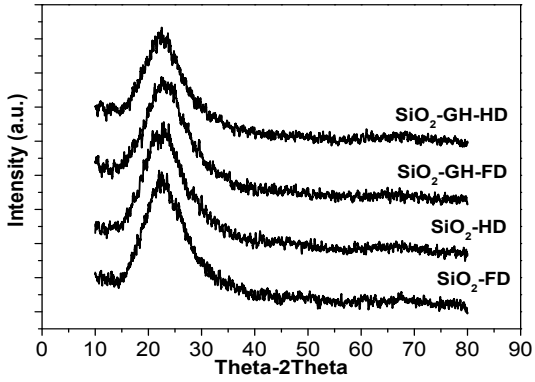

Figure 4. X-Ray diffraction patterns of the investigated samples

The results of DLS analysis show that the size is a little bit larger for the unloaded than for silica samples loaded with GH, as a consequence of increased matrix shrinkage and increased endurance to grinding, in the absence of GH, mainly caused by the increased gelling time of sols in the absence of GH (Table 3). Having in view that the nanoencapsulation of pharmaceutically active natural compounds involves drug-loaded particles with diameters ranging from 1 to 1000 nm [11], the particle sizes (Table 3) suggest that GH is nanoencapsulated in the silica microparticles (nano in micro). A slightly higher negative charge value is observed for SiO_2-FD compared to SiO_2-HD (Table 3) because the freeze drying leads to more hydroxylated silica samples as a consequence of a faster rate of the hydrolysis against the condensation reactions. Highly hydroxylated silica induces high density of $Si\text{-}O^-$ groups in neutral-basic pH medium. The density of negative charges on the silica surface is higher in pure samples compared to GH encapsulating silica, which proves the GH loading since a part of the silanol groups are linked through hydrogen bonds to organic compounds from GH. The difference in zeta potential values between loaded and unloaded samples is smaller for SiO_2-FD particles compared to SiO_2-HD) due to a decreased attachment of silanol groups to organic compounds from GH, during the freeze drying process, or due to other chemical interactions, difficult to be identified, between some compounds from GH (degradation compounds) or between GH and silica matrix that can bring changes in zeta potential values.

Table 3. Size and zeta potential values of the synthesised particles

	SiO_2-HD	SiO_2-GH-HD	SiO_2-FD	SiO_2-GH-FD
Size (µm)	1,2	1	1,1	1
Zeta potential (mV)	-32.7	-12.3	-37.6	-20.7

In the DTA curves (Figure 5) occurs an endothermic peak around 90-100°C, corresponding to the removal of surface water and solvents used in samples synthesis, accompanied by a drastic weight loss of 10-20%. In the bare samples, the second weight drop, above 100°C corresponds to the release of the water remained in pores, degradation of residual starting materials, dehydroxylation due to the condensation of OH groups in the silica particles and to silane groups of the xerogel condensed to siloxanes. The number of hydroxyl groups in silica, n_{OH}, can be determined by thermogravimetry [12]. The results obtained for our samples are 10.55 and 6.88 mM/g SiO_2 for SiO_2-FD and SiO_2-HD, respectively showing that SiO_2-FD samples are more hydroxylated compared to SiO_2-HD, and they confirm the results obtained by zeta potential measurements. The exothermic event around 440°C in SiO_2-FD bare samples is probably caused by a restructuration of the matrix through an incipient crystallization process. For the GH encapsulating samples, the decomposition of the organic compounds begin around 150°C and corresponds to the 150°C to 650°C endothermic events observed in DTA runs. In this temperature range, by comparing TGA curves of bare samples with those of the loaded ones, it can be seen that the total weight loss for samples with plant extract is higher than that for the bare samples, and this proves the incorporation of organic compounds inside silica matrices (Table 4).

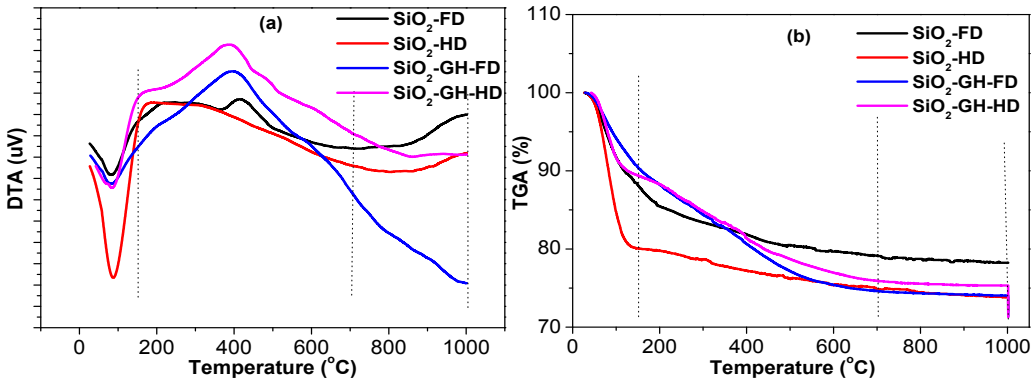

Figure 5. DTA (a) and TGA (b) diagrams of the investigated samples

Table 4. Weight loss percent during TGA analysis for investigated samples

Temperature range → Sample ↓	20-150°C	150-650°C	650-1000°C
SiO_2-FD	12%	8.3%	1.2%
SiO_2-GH-FD	9.8%	15.3%	0.9%
SiO_2-HD	19.9%	4.8%	1.4%
SiO_2-GH-HD	10.6%	12.9%	1%

FT-IR spectra reveal specific absorbance bands for bare and loaded particles (Figure 6). Majority of the identified bands correspond to silica matrix.

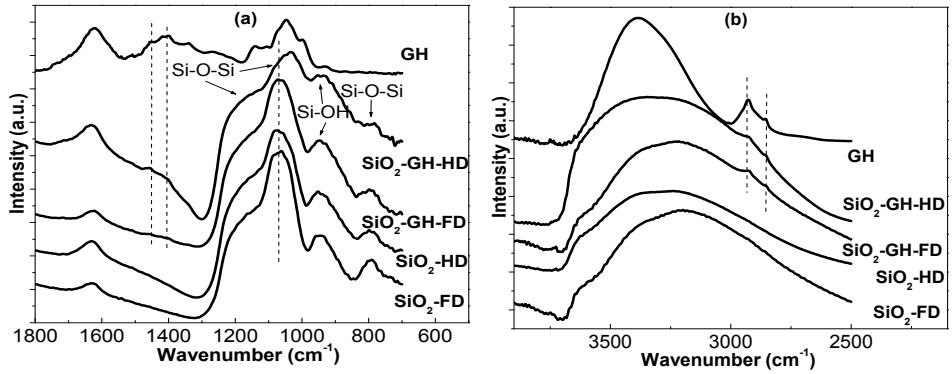

Figure 6. FT-IR spectra of the investigated samples in (a) 700-1800 cm^{-1} and (b) 2500-4000 cm^{-1} ranges

Silica matrices with GH present minor changes in FT-IR spectra. In the spectra of GH loaded samples are also present specific bands at 2928, 2845, 1453 and 1400 cm^{-1} characteristic to GH. Furthermore, the presence of multiple hydrogen bonds, evidenced by the vibration bands from 3450 cm^{-1} (Figure 6), also confirms the GH encapsulation in silica microparticles [13]. The GH characteristic bands at 1045 and 990 cm^{-1} are more evidenced in SiO_2-HD than in SiO_2-FD due to the fact that during heat drying an intense shrinkage of the matrix occurs, causing a higher quantity of GH per silica volume unit compared to SiO_2-FD sample.

Analysis by UV–Vis spectroscopy (Figure 7) showed a broad band around 560 nm appears in GH encapsulating silica irrespective of the drying route. This band could be assigned to aromatic compounds with chromophores of some OH multiple bonds originated from polyphenols [13] to organometallic complexes that can be also present in the extract and whose "d" electrons could be excited from one electronic state to another or as a consequence of the formation of new compounds. This band is better emphasized for SiO_2-GH-HD than for SiO_2-GH-FD particles because the higher drying temperatures and

longer drying periods, along with the shrinkage of the silica matrix promote an increase in chromophores groups formation.

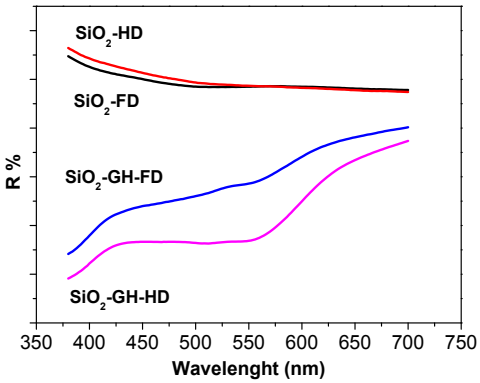

Figure 7. UV-Vis DRS spectra of the investigated samples

The typical fluorescence spectrum of alcoholic extract from cotton seeds plants appears in 350 - 700 nm range with two maxima of fluorescence located at about 420 and 460 nm (insets of Figure 8a,b). This fluorescence is caused by the outer pigment layer of the cotton seed coat which contains polyphenols like anthocyanin, roanthocyanidin compounds [14] or from other compounds.

Pure silica (SiO_2-HD and SiO_2-FD) particles excited at 260 nm present an unexpected fluorescence emission band around 300 nm (Figure 8a) that seems to be partially perceived also under 300 nm excitation (Figure 8b). Previous studies on silica have suggested that the fluorescence sources in the UV-B range are nanosized hydrogen-passivated silica species [15]. This nanoparticulation seems to be more pronounced during freeze drying, because the fluorescence observed for the freeze dried silica is slightly higher compared to heat dried silica.

The fluorescence emission at around 300 nm decreases by loading of silica particles with GH, while the fluorescence centred around 440 nm, specific to GH, is pronouncedly amplified as the plant extract is loaded in the silica particles probably due to prevention of self-quenching by homogeneous distribution of the fluorescent GH into the silica matrix [13]. The diminishing of the fluorescence recorded from unloaded silica particles may be caused by some molecular interactions like excited-state reactions, molecular rearrangements, energy transfer, ground state complex formation or collisional quenching [16].

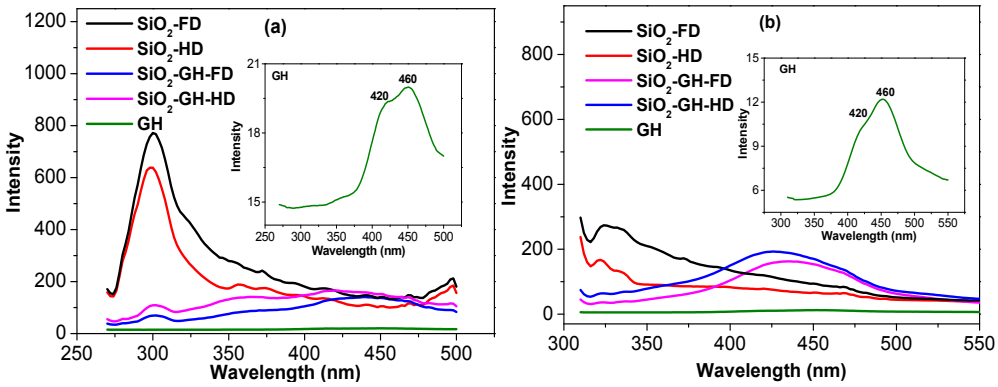

Figure 8. The fluorescence spectra of investigated samples at different wavelength excitation: 260 nm (a), 300 nm (b)

The release profiles for SiO_2-GH-FD and SiO_2-GH-HD (Figure 9a) at pH 1.1 and at pH 7.4 values show an initial burst release in the first 4 h (Figure 9b) followed by a slower release period for the next 140 h, so that in both cases the release kinetics is biphasic.

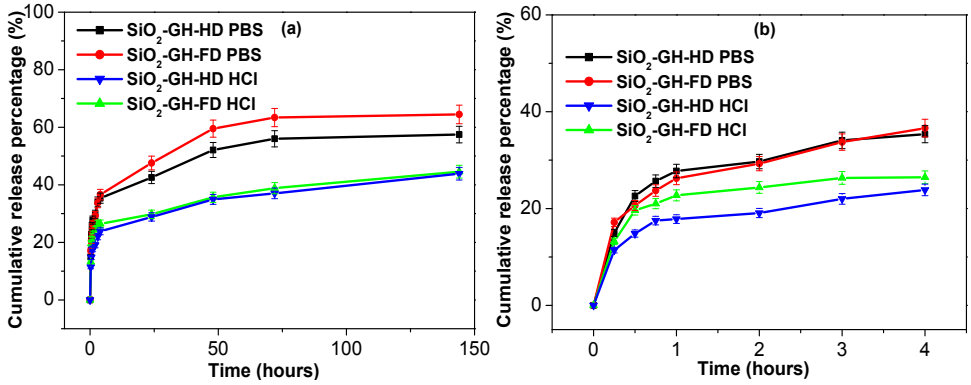

Figure 9. The *in vitro* release profile of *Gossypium hirsutum* extract from prepared samples in different pH media for the whole time interval (a) and for the first 4 h (b)

The release is slower from SiO_2-GH-HD than from SiO_2-GH-FD particles due to the fact that during heat drying an intense shrinkage of the matrix occurs, compared to the freeze drying process [17]. Beside a slower release this implies a stronger binding of GH compounds inside silica matrix, fact also proved by zeta potential and DTA/TGA measurements, through a decreased number of Si-OH groups in heat dried samples. The higher release at pH 7.4 may be due to electrostatic interactions repulsion between compounds from GH and silica matrix [18, 19], because zeta potential at the silica surface changes as the silanol groups on the surface are protonated or deprotonated depending mainly on the solution's pH.

The *in vitro* release data were analysed through different kinetic models to understand the mechanism of drug release (Table 5). According to Korsmeyer-Peppas

equation, (log cumulative percentage of drug released versus log of time). The slope values (n values) ranged from 0.16 to 0.27 (n<0.45) and point out that the drug release follows a very slow quasi-Fickian diffusion, useful in the design of pellets and coatings for controlled release [19, 20].

Table 5. GH release kinetic constants from silica matrix

Sample	Zero-order (R^2)		First-order (R^2)		Higuchi's plot (R^2)		Korsmeyer-Peppas model			
							(R^2)		n value	
	4h	140h	4h	140h	4h	140h	4h	140h	4h	140h
SiO_2-FD PBS	0.931	0.596	0.948	0.628	0.981	0717	0.991	0.817	0.267	0.168
SiO_2-HD PBS	0.791	0.654	0.825	0.636	0.887	0.770	0.909	0.859	0.279	0.168
SiO_2-FD HCl	0.689	0.922	0.712	0.942	0.810	0.976	0.862	0.993	0.223	0.224
SiO_2-HD HCl	0.862	0.942	0.877	0.958	0.927	0.982	0.947	0.991	0.240	0.229

We have to outline that the release process along with the composition of the GH is a complex one. Chemical structure of nonentrapped GH was characterised by FT-IR in terms of drying temperature, and some minor chemical changes in flavonoids, isoprenoids and carbohydrates structure were observed (Figure 3). We considered important to check if similar changes take place during drying inside silica matrices, but FT-IR spectraof GH entrapping silica are dominated by absorbance bands mainly characteristic to silica (Figure 6). Therefore we decided to investigate by FT-IR spectroscopy the GH released from SiO_2-GH-FD and SiO_2-GH-HD samples in water to see if there are some structural changes in composition of nanoencapsulated GH after thermal treatment (Figure 10). To specify that for FT-IR measurements, the GH released in water solutions were dried.

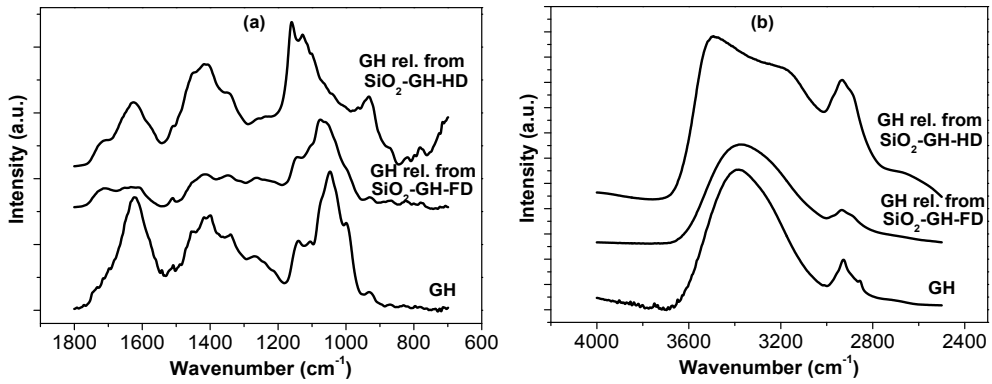

Figure 10. FT-IR spectra of the dried released GH from SiO_2-GH-FD and SiO_2-GH-HD samples in water in (a) 700-1800 cm^{-1} and (b) 2500-4000 cm^{-1} ranges

The main differences between the GH released from differently treated matrices (Figure 10) occur in the spectral range between 700 and 1800 cm^{-1}. In the spectrum of GH released from freeze dried particles one notices a decrease of 990 cm^{-1} absorption band, and this denotes a change of carbohydrates chemical composition, as well as the appearance of a new band around 1720 cm^{-1} denoting a saturation of ketone/aldehydes, resulting in aliphatic ketone/aldehydes. Heat and freeze drying routes lead to different spectral changes for the GH released from silica matrix compared to nonentrapped GH. These changes are evidenced by C-O stretching vibrations from carbohydrates and C-H bending vibrations from isoprenoids; they indicate that the encapsulation influences the organic compounds entrapped inside, but it is difficult to assume how their therapeutic properties would be affected.

2.4. Conclusions

Gossypium Hirsutum seeds extract was successfully nanoencapsulated in silica microparticles with average diameter close to 1 μm by sol–gel method using heat drying and freeze drying. Silica nanoparticulation was also highlighted by the results obtained through fluorescence spectroscopy, mainly in case of freeze dried samples. The evidence of plant extract entrapment and structural information were obtained through TG/DTA, FT-IR, UV-Vis-DRS and fluorescence spectroscopy. The drying process influences both the silica host microparticles and the plant extract. The amorphous structure of the system tested along with its enhanced fluorescence properties may lead to future biomedical applications as fluorescent labels for cells, especially if the system is configured at nanometric sizes and/or functionalised with targeting ligands. The release profiles of the entrapped plant extract showed biphasic profile and presented a more pronounced sustained release for heat dried samples than for the freeze dried ones. The amount released was increased in 7.4 pH medium compared to 1.1 pH medium, regardless of the drying process used in synthesis. Future *in vitro* studies regarding their toxicity and therapeutic effects can be considered. These results support the idea that silica particles nanoencapsulating *Gossypium hirsutum* extract can be further considered for application in fluorescence microscopy or sustained therapy taking into consideration its possible pharmacological properties.

3. SILICA-GADOLINIUM PARTICLES LOADED WITH GOSSYPOL FOR SIMULTANEOUS THERAPEUTIC EFFECT AND ENHANCED MRI CONTRAST AGENT

3.1. Main objectives

The incorporation of gossypol, a polyphenolic compound with a broad spectrum of therapeutic properties, in a porous gadolinium-silica matrix was considered for both therapeutic effect and contrast in magnetic resonance imaging. The purpose of this study was to evaluate gossypol loading on silica-gadolinium microparticles prepared at two different pH values, as the first step in designing new theranostic (therapeutic and diagnostic) compounds.

3.2. Synthesis and characterization methods

The $98SiO_2 \bullet 2Gd_2O_3$ (mol %) system was prepared by sol-gel process at two different pH values (2 and 5.5). The wet gels were placed in cryovials, freezed in liquid nitrogen (FD) for 20 min and thawed to room temperature. The wet samples were dried at 110 °C for 1 hour and then grounded to a fine powder using an agate mortar and pestle, and thermally treated at 500°C in air for 30 min. For gossypol loading, 100 mg of each silica gadolinium powder were immersed in 2 ml acetone containing 4 mg of gossypol (Gos, $C_{30}H_{30}O_8$, Sigma Aldrich). The mixtures were kept at 4°C for 48 h and then the supernatant was removed after centrifugation. The remained samples (noted FD2-GOS and FD5.5-GOS) were left to dry at 37 °C. The structure of the particles and their loading with gossypol were investigated by XRD, DLS, BET/BJH analysis, DTA/TGA, FT-IR, EPR and XPS. The potential applications in MRI of silica-gadolinium particles loaded with gossypol were tested through MRI measurements.

3.3. Results and discussion

The XRD patterns (Figure 11) recorded before and after gossypol loading indicate a prevalent amorphous state in all samples. It is desirable to have amorphous phases since amorphous silica particles are considered less toxic than the crystalline ones [9] and, on the other hand, amorphous drugs have a higher saturation solubility than the crystalline forms [21].

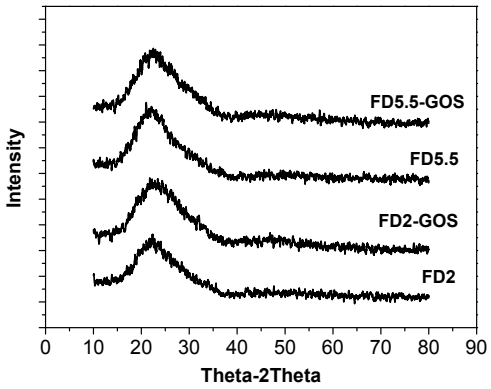

Figure 11. XRD patterns of investigated samples

The DLS measurements showed that the medium particles size ranged from 0.90 μm to 1.05 μm. The drug loading process slightly affects the particles size. After Gos loading the sample prepared at pH 2 presents a light size increase, compared to the sample prepared at pH 5.5 that could indicate a higher loading of Gos on samples prepared at lower pH. The zeta potential values for the Gos loaded samples are outside the ±30 mV range denoting the possibility to avoid particles aggregation and thereby they can be physically stable in suspensions. Since Gos is negatively charged [22, 23], the particles loading with Gos increases the negative value of their superficial charge. This process is better evidenced for the FD2 samples and suggests a higher Gos loading than for FD5.5 sample. The Gos may be physically adsorbed but also chemically bound to the samples [24].

The BET analysis shows that both specific surface area and pore volume decrease after Gos loading. This decrease is more pronounced for the FD2 samples, in agreement with the results obtained by particle size and zeta potential analysis and supports the assumption that more Gos is loaded in the samples prepared at lower pH values.

The thermal curves for pure Gos (inset of Figure 12b) show an endothermic reaction at around 180°C and ~5,8 % weight loss which might be due to the melting process with partial decomposition, Gos melting point being around 180-214°C [25], followed by a well outlined exothermic reaction from 450-600°C with ~63% weight loss, corresponding to Gos decomposition into gases like CO_2 and/or CO and H_2O as a consequence of combustion.

The DTA curves for FD2 and FD5.5 samples present two main regions of thermal events and correspond to two main regions of weight loss (Figure 12). The weight loss before 200°C, with an endothermic peak in DTA traces can be associated with the removal of surface adsorbed water molecules as well as of ethanol or acetone remains from

synthesis. A part of the weight loss at around 180°C, for FD2-Gos and FD5.5-Gos samples is due to partial decomposition of Gos during its melting. Further weight losses correspond to dehydroxylation of silica matrices and decomposition of Gos. It has to be outlined that including Gos in silica pores could improve its thermal stability, as occurs in Gos inclusion in β-cyclodextrine [26]. The weight loss percent differences between the loaded and unloaded samples, in the 20-800°C temperature range, are 3.1% and 2.8% for FD2 and FD5.5 samples, respectively, which corresponds to the loading of 3.1 mg and 2.8 mg of Gos on 100 mg of FD2 and FD5.5 samples proving that FD2 particles are incorporating a higher quantity of Gos.

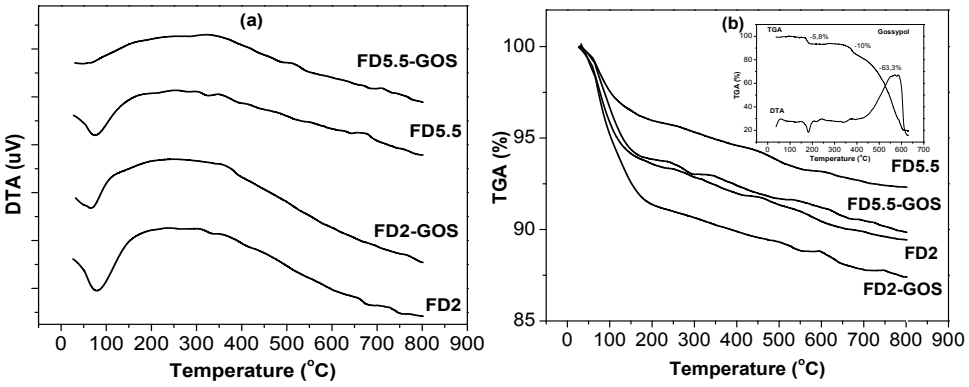

Figure 12. DTA (a) and TG analyses (with inserted gossypol DTA/TGA curves) (b) for investigated samples

Table 6. Percent weight loss from TG analyses

Temperature (°C)	FD2 (%)	FD2-Gos (%)	FD5.5 (%)	FD5.5-Gos (%)
20-200	6,7	10	4,4	7
200-800	4,1	3,9	3,7	3,9

The Gos loaded silica-gadolinium particles FT-IR spectrum contains most of the major absorption bands of pure silica-gadolinium particles and no noticeable new bands specific to Gos are observed.

The FT-IR spectra recorded for Gos and for the supernatant acetone solution recovered from silica-gadolinium particles were further analysed to obtain more information regarding Gos spectral features after its inclusion into silica-gadolinium particles. In the 3800-3100 cm^{-1} spectral range, the FT-IR spectrum of the initial Gos solution in acetone (Figure 13a) displays only a narrow peak at around 3500 cm^{-1} assigned to hydroxyl groups involved with different strength in the hydrogen bonds formation, specific to aldehyde tautomer structure [27-32], and a broadened one at around 3420 cm^{-1}.

Both bands are present in the FT-IR spectra of both Gos recovered solutions, but the band at 3420 cm^{-1} is significantly broadened in the FD5.5 recovered solution. This is due to the presence of Na^{+} in FD5.5 samples; aldehyde tautomer of Gos tends to change into ketone tautomer with a specific broad band at around 3420 cm^{-1} [29].

In the spectral region from 1700 to 1500 cm^{-1} (Figure 13b), the FT-IR spectra of Gos and FD2 recovered solution present aldehydic tautomer specific vibration bands at around 1615 cm^{-1}, assigned to C=O bonds, and around 1570 cm^{-1} specific to C=C naphthalene ring vibrations. The FD5.5 recovered solution shows vibration bands specific to ketone tautomer; the band from 1570 cm^{-1} decreases and a new band at 1595 cm^{-1} appears, which is specific to ring vibrations from ketone tautomer [29].

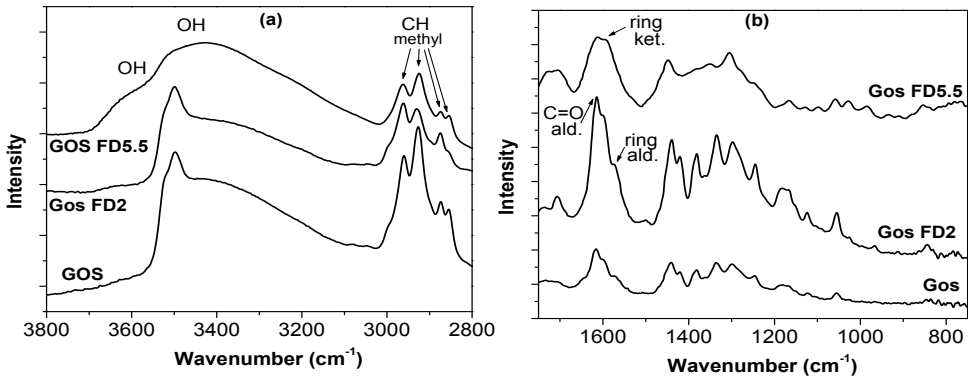

Figure 13. FT-IR spectra of recovered supernatant Gos solutions for different spectral ranges: (a) 3800-2800 cm^{-1}, (b) 1800-700 cm^{-1}

The X-band EPR spectra (Figure 14) present features at the effective g-values g_{eff}=5.9, 2.8 and 2.0, characteristic to the so-called U-spectrum, typical for Gd^{3+} ions disposed in different sites, where they experience a relative weak crystalline field, and are characterised by a coordination number higher than six [33]. Since the FD5.5 and FD5.5-Gos samples present spectral features more broadened than in the FD2 and FD2-Gos samples, we expect higher clusterization degree of the Gd^{3+} ions in the FD5.5 samples compared the FD2 samples, due to the increased condensation reaction rate with increasing pH synthesis condition [34].

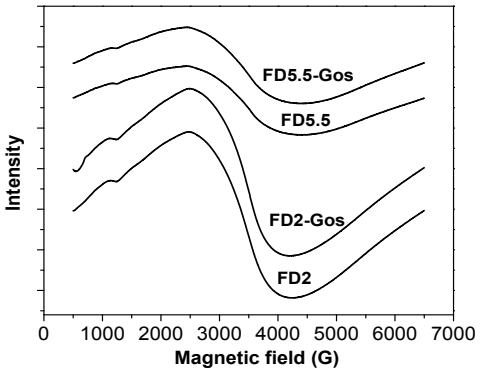

Figure 14. Experimental EPR spectra of investigated samples 500-6500G

Comparing the theoretical elemental composition with that obtained through XPS analysis (Table 7), it can be observed that atomic percentage on samples surface is lower than expected and this is due to the clusterization of gadolinium mainly inside of the particles.

Table 7. Relative percentage of the main components compared with theoretical composition

	Elemental composition (at %)		
	O	**Gd**	**Si**
FD2	59.8	0.2	40.0
FD5.5	58.7	0.2	41.1
Theoretical composition	66.5	1.3	32.2

The relative atomic concentrations of the samples before and after the immersion are presented in Table 8. The content of carbon increased significantly, especially for the Gos loaded samples prepared at pH 2.

Table 8. Relative percentage of the main components before and after Gos loading

	Elemental composition (at %)			
	Si	***Gd***	***C***	***O***
FD2	39.4	0.2	1.7	58.7
FD2-Gos	35.4	0.2	10.4	54.0
FD5.5	40.7	0.2	1.0	58.1
FD5.5-Gos	40.0	0.2	2.2	57.6

Before immersion in Gos solution, the O 1s photoelectron peak consists of a main component at 533.2 eV, related to the bridging oxygen atoms involved in the structural units of the silica matrix [35] and a shoulder at higher binding energies corresponding to hydroxyl groups [36], which is better outlined in FD2 samples compared to FD5.5 samples due to a high hydroxylation of silica matrix as a consequence of increased condensation reaction rate at higher pH synthesis conditions [34, 37]. After loading with Gos, in the outermost atomic layer of the FD2-Gos sample is observed a decrease in O 1s peak

intensity and a high similarity to oxygen photoelectron peak of Gos (Figure 63), while in the outermost layer of FD5.5-Gos sample are further well evidenced the oxygens of silica matrix, as reflected for FD5.5 sample (Figure 15). The results outline again a higher Gos payload on FD2 samples.

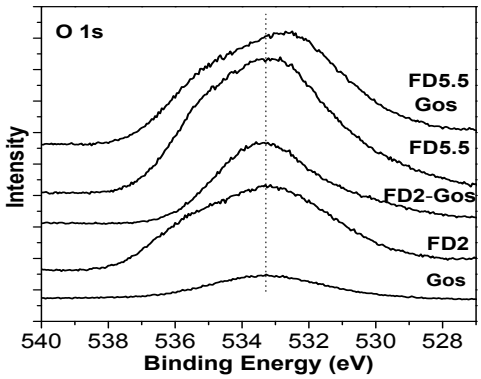

Figure 15. High-resolution XPS spectra recorded for O_{1s}

Gadolinium binding on the surface of silica pores, causes a reduction of its characteristic rotational correlation time, and thereby causes shorter T_1 relaxation time values. A higher clusterization in FD5.5 samples compared to FD2 samples diminishes the ability of paramagnetic centres to induce water relaxation and leads to a longer T_1 for FD5.5 samples compared to FD2 samples (Figure 16). After particles loading with Gos, the outer sphere of gadolinium oxide changes in improving the relaxivity, FD-Gos samples presenting a shorter T_1 values than FD samples. The contrast in MR images (Figure 17) is improved for particles loaded with Gos, compared with the pristine silica-gadolinium particles. This could happen because strong hydrogen bonds are formed between carbonyl and hydroxyl groups of Gos with water that increases second sphere involvement in relaxivity process. Anyway, we should not rush to conclusions, and to take into account further studies and measurements to determine not only relaxation time but also the relaxivity values, which are appropriate parameters to evaluate contrast agents' capability to induce proton relaxation.

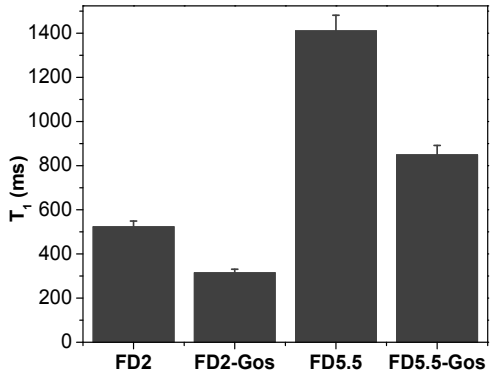

Figure 16. T_1 relaxation times of samples before and after Gos loading

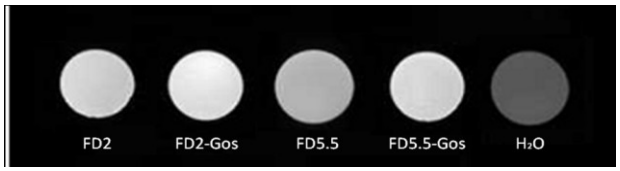

Figure 17. T_1-weighted phantom MR image of silica-gadolinium particles and water at 7 T by the spin-echo method with TR/TE =1300 ms/9 ms, FOV =2 cm, NEX=1; BW=70 000 Hz, slice thickness=1.00 mm, matrix =256 × 256, and temperature = 20 °C

3.4. Conclusions

Silica particles doped with gadolinium were prepared by sol–gel method at two pH values, and loaded with Gos. The Gos loading slightly affects the particles size kept close to 1 μm. A higher amount of Gos is loaded in the sample prepared at pH 2 than in the sample prepared at pH 5.5. The FT-IR results obtained on recovered Gos solution indicate that Gos remains in its aldehyde tautomer structure in the sample prepared at lower pH, while in the sample prepared at higher pH a shift to ketone tautomer structure occurs. EPR and XPS analyses show that gadolinium ions tend to concentrate inside the particles and to form clusters, especially in the sample prepared at pH 5.5. The MRI measurements reveal the shorting of T_1 relaxation time as the gadolinium doped silica particles are loaded with Gos. These results offer appropriate characteristics to further study Gos loaded silica-gadolinium particles as MRI contrast agent and theranostic compound.

4. DUAL-FUNCTIONAL SILICA-GADOLINIUM NANOPARTICLES EMBEDDED WITH GOSSYPOL ACETIC ACID AS THERANOSTIC COMPOUNDS

4.1. Main objectives

In this study, dual functional silica nanoparticles containing gadolinium and gossypol acetic acid were investigated in order to assess their possible development as theranostic compounds, with anticancer properties from gossypol acetic acid and with MRI capabilities from gadolinium. In subchapter 4.2, it was evaluated gossypol loading on two types of silica-gadolinium microparticles prepared at two different pH values and offered favourable results regarding relaxation times values of microparticles. Therefore our aim in this study was to obtain similar but nanosized compounds which are capable of passive targeting as a consequence of their reduced sizes and vascular enhanced permeability effect at the tumour tissue level.

4.2. Synthesis and characterization methods

The silica-gadolinium nanoparticles (SiGd-NPs, $98.4SiO_2 \cdot 1.6Gd_2O_3$ (mol %)) were prepared by sol-gel method using surfactants and polymers as template. Contrary to the results presented in Subchapter 4.2, it was chosen to synthesise the nanoparticles in a basic medium, because this type of synthesis was the most common method encountered in literature for nanosized SiGd-NPs, and we considered the increase of specific surface area, porosity along with drug concentration and repetition of loading plus sonication sufficient to increase drug upload. The fine-particle precipitates were collected, freeze dried and then calcinated at 550°C in air for 5 h to remove the templates. Gossypol acetic acid (GosAa) molecules were loaded on SiGd-NPs pore and surface by simple immersion. For an enhanced loading, at 24 h interval, particles were sonicated in water bath for 1 hour at 200 W, centrifuged, the supernatant was removed, freeze dried and immersed again in solution of GosAa. For relaxometry and *in vitro* studies, in order to obtain more stable suspensions in terms of time of suspension, samples were placed with sonication in a viscous solution of carboxymethylcelullose (CMC, 2%, Sigma Aldrich) in phosphate buffer (PBS, pH 7.4).

These nanoparticles (NPs) were characterized by SEM, TEM, EDX, DLS measurements, XRD, BET surface area analysis, BJH pore volume analysis, TGA and FT-IR spectrometry. Capabilities of SiGd-NPs to be employed also as contrast agents were determined from their NMRD profiles and by a 7 T MRI uptake *in vitro* experiment.

Likewise, release studies characterised by kinetics models and cytotoxicity studies were performed.

4.3. Results and discussion

SEM micrographs of synthesised nanoparticles (Figure 18) show agglomeration of spherical shaped, nanometric sized, of around 100 nm particles. Moreover the atomic percentage of the main components obtained from EDX spectra are in good correlation with the ones calculated from the synthesis formula.

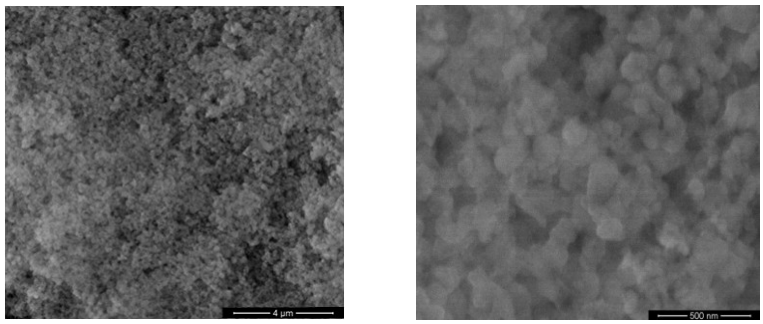

Figure 18. SEM micrographs of SiGd-NPs at two different magnification

HRTEM image of SiGd-NPs (Figure 19) revealed the amorphous structure of the matrix with the presence of the Gd assembled in silica matrix (dark spots), as proved by EDX spectrum.

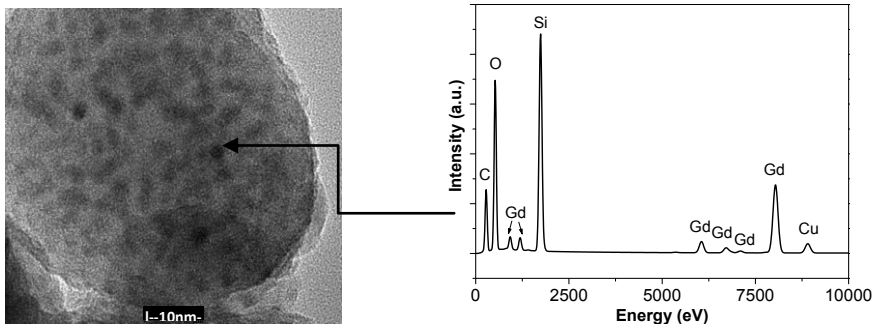

Figure 19. HRTEM image and EDX analysis of single particle of SiGd-NPs

DLS measurements showed sizes less that 350 nm after sonication, these nanoparticles being theoretically capable of taking advantage of the leaky vasculature and poor lymphatic drainage system of tumours to enhance the retention time of drug, the so called passive targeting [38].

GosAa salt loading on SiGd-NPs does not bring significant changes in zeta potential values. In both cases, zeta potential values were close to -30 mV, resulting in relative stable nanosuspensions (Table 9) [21].

Table 9. Sizes and zeta potential values of the investigated samples

	Average size (nm)	Zeta potential (mV)
SiGd-NPs	294	-24,5
SiGd-NPs-GosAa	340	-26,4

XRD analyses (Figure 20) confirm the amorphous structure of silica-gadolinium sample revealed also by HRTEM, indicating also that GosAa loaded is present in an amorphous state after the loading process. It was proven that encapsulation of amorphous and hydrophobic drugs in porous inorganic systems induce enhancement of its dissolution process [39]. Dissolution of poorly water-soluble drugs represents the rate-limiting step for therapy. That is why it is important to improve the dissolution rate and thus enhance drug bioavailability.

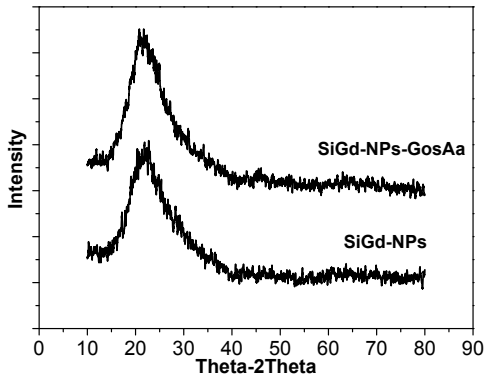

Figure 20. XRD patterns of the SiGd-NPs before and after GosAa loading

Pore volume and surface area analysis showed that SiGd-NPs present a high specific surface area and a large pore volume (around 600 m^2/g and 0.6 ml/g, respectively), being suitable as a carrier for drug molecules in a sustained drug-release system. GosAa loading on silica-gadolinium nanoparticles surfaces causes the decrease of NPs surface area and pore volume.

TGA curves presented in Figure 21 show two mass loss steps from 20 to 200°C attributed to the thermo desorption of physically adsorbed water or other solvents used in synthesis and from 200 to 800°C induced by the decomposition of residual organic templates used in synthesis, dehydroxylation of Si-OH [40] or Gd-OH [41], and in case of GosAa loaded samples generated by the decomposition and combustion of organic drug. The weight loss in Si-Gd-NPs-GosAa samples is higher compared to SiGd-NPs samples, which proves drug loading on pores and surface of NPs. The weight loss percent differences between the loaded and unloaded samples, in the 20-800°C temperature range,

is 10%, which corresponds to the loading of 10 mg of GosAa on 100 mg of SiGd-NPs samples.

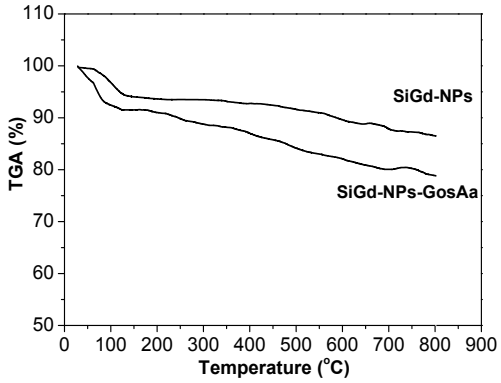

Figure 21. TGA of the investigated samples

Figure 22 shows the FT-IR spectra of the loaded and unloaded sample as well as the pure GosAa spectrum. Most of the vibrational bands identified correspond to silica matrix. It can be noticed that SiGd-NPs-GosAa samples present minor specific vibrational bands of GosAa at around 1450 cm^{-1} and at around 2920 cm^{-1} corresponding to C-C, C=C stretching vibration bands and to C-H stretching vibration from methyl groups, respectively [32]. Furthermore, the slightly increased intensity of the broad band from around 3400 cm^{-1} and the one from around 1640 cm^{-1}, could confirm GosAa loading on silica-gadolinium nanoparticles surfaces.

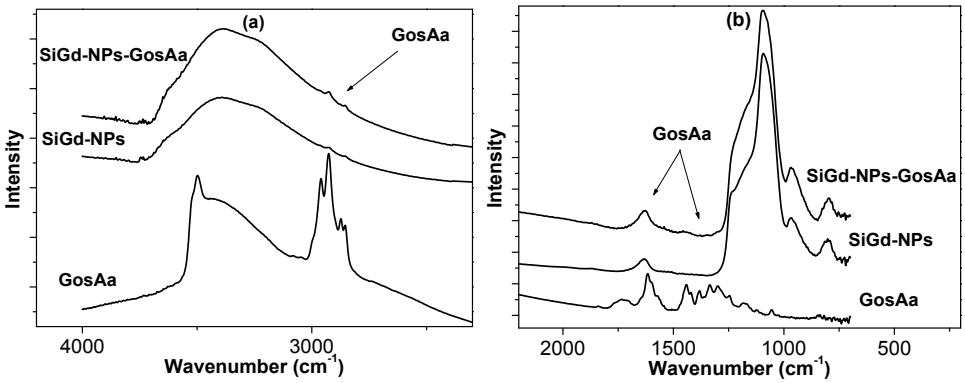

Figure 22. FT-IR spectra of GosAa and investigated samples

NMRD profiles of investigated samples are shown in Figure 23. The high peak centred at around 30 MHz is characteristic of Gd ion bonded to macromolecules. There are some studies showing that Gd_2O_3 is strongly bonded to silica matrix, that behaves like a macromolecule, slowing its rotational tumbling and by consequence increasing its relaxivity properties as contrast agent used in MRI [42, 43]. This strong bonding can also suggest that Gd_2O_3 molecules or Gd ions hardly can dissociate from the silica matrix. That

is why gadolinium-silica nanoparticles present theoretically no toxicity and by its porous structure can offer access of water molecules to Gd paramagnetic centre [44].

Withal, NMRD experiment data (Figure 23) indicates that GosAa loading on the SiGd-NPs surfaces and pore increases its relaxation rate over the entire frequency range investigated, although SiGd-NPs-GosAa shows higher sizes compared to SiGd-NPs, and its relaxivity should theoretically decrease [45]. We can assume that the observed increased relaxivity in case of GosAa loaded samples was influenced by the increased hydrogen bonds, interfaced by gossypol acetic acid, between water molecules and the polar groups present in the second or outer sphere coordination sphere of Gd ions [46-48].

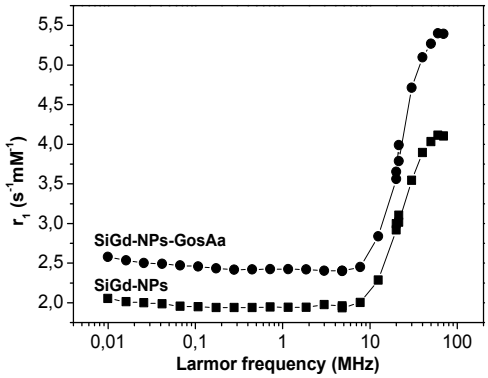

Figure 23. NMRD profile of SiGd-NPs and SiGd-NPs-GosAa in CMC 2%

Loading of drug into a porous system causes a sustained release of the drug when immersed in biological fluids, minimising thereby its side effects (Figure 24).

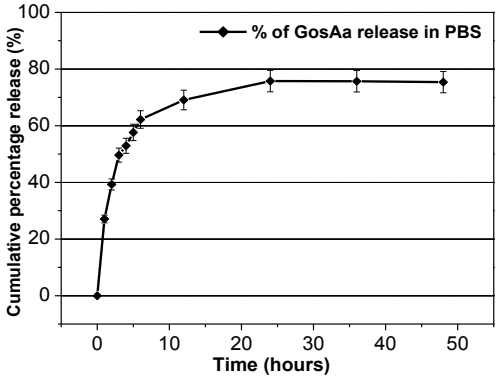

Figure 24. Release profile of GosAa from SiGd-NPs-GosAa

The kinetic model that best matches the release data was evaluated through correlation coefficient (R^2). Plotting according to a first-order equation, the formulation showed a low linearity, with regression values of 0.936. The best match with correlation values higher than 0.98 was found with the Korsmeyer-Peppas model, that showed slope values less than 0.5 ($n<0.5$), indicating that drug release mechanism from the nanoparticles was controlled by diffusion [49, 50].

As can be observed from cytotoxixity studies (Table 10), an acceptable viability value higher than 80% was obtained for all concentration, the toxicity increased with increasing Gd and GosAa concentrations ({Gd}, {GosAa}). There was a slight difference between cells incubated with SiGd-NPs and blank which suggests that SiGd-NPs did not significantly affect cell viability at the tested concentrations over 6 hours in cell culture. Once GosAa is loaded into silica-gadolinium nanoparticles, toxicity effect on cells slightly increased, fact anticipated due to anticancerous activity of GosAa. Slight decrease in toxicity for SiGd-NPs-GosAa samples compared to pure GosAa could be also observed, denoting a decreased cytotoxic effect of SiGd-NPs-GosAa due to the sustained release of the drug from silica-gadolinium nanoparticles.

Table 10. Cytotoxicity studies on TSA breast cancer cells

Samples	**Viability (%)**	**Samples**	**Viability (%)**	**Samples**	**Viability (%)**
Blank	100				
SiGd-NPs		**SiGd-NPs-GosAa**		**GosAa**	
{Gd} 20μM	97	{Gd} 20μM {GosAa} 0.72μM	93	{GosAa} 0.72μM	91
{Gd} 50μM	95	{Gd} 50μM {GosAa} 1.72μM	89	{GosAa} 1.72μM	87
{Gd} 100μM	93	{Gd} 100μM {GosAa} 3.47μM	85	{GosAa} 3.47μM	84

To evaluate the amount of SiGd-NPs taken up by TSA breast cancer cells after 6 hours incubation, Gd ion concentration was measured by Inductively Coupled Plasma mass spectrometry (ICP-MS) analysis. The results show that the amount of Gd associated with TSA cells is directly proportional to the loading amount of SiGd-NPs in the cell media (Figure 25). Small differences were observed between SiGd-NPs and SiGd-NPs-GosAa, seeming that by loading GosAa on nanoparticles the percent concentration of uptaken nanoparticles by TSA cells slightly increases.

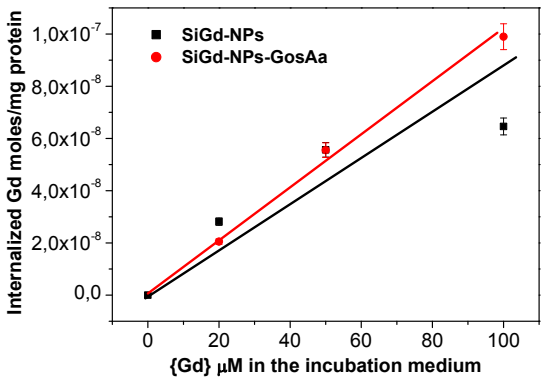

Figure 25. Loaded and unloaded SiGd-NPs (express in Gd moles) uptaked in TSA cells after 6 h incubation at 37°. The amount of cell associated Gd has been determined by ICP-MS.

T_1 and T_2 weighted images of glass capillaries containing cellular pellets obtained by incubating about $2{,}4\times10^6$ TSA cells with increasing amounts of loaded and unloaded nanoparticles were acquired at 7 T (Figure 26). As can be observed, the T_1 values are slightly decreasing along with the nanoparticles concentration (Table 11), results that are in accordance with the ICP-MS measurements from uptake experiment. The recorded T_1 values of the cells incubated with SiGd-NPs-GosAa are slightly different compared with the non-loaded ones, but notably different from the blank sample (Figure 26), denoting the fact that cells manifest an adequate uptake of silica-gadolinium nanoparticles and an appropriate contrast effect to be used as magnetic resonance contrast agents. We could not observe the decrease of T_1 values in cases of GosAa loaded samples, as should be expected from uptake experiment and ICP-MS measurements, but we have to take into consideration the artifacts presence in MRI image acquisition, which can affect measurements of T_1 values.

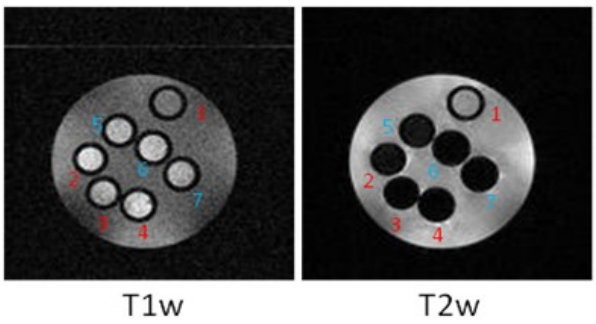

Figure 26. T_1 and T_2 weighted spin echo images, recorded at 7 T, of an agar phantom containing capillaries with pelleted TSA cells. (1) non-incubated control cells. (2), (3) and (4) incubated cells for 6 h with unloaded nanoparticles of 20, 50 and 100 µM Gd concentration, respectively. (5), (6) and (7) incubated cells with loaded nanoparticles of 20, 50 and 100 µM Gd concentration, respectively

Table 11. T_1 and T_1 decrease percentage values measured at 7 T of pelleted TSA cells

Sample	T_1 (ms)	T_1 decrease (%)	Sample	T_1 (ms)	T_1 decrease (%)
(1) Control cells	2467				
SiGd-NPs			**SiGd-NPs-GosAa**		
(2) {Gd} 20μM	961	61	**(5)** {Gd} 20μM	1103	55
(3) {Gd} 50μM	640	74	**(6)** {Gd} 50μM	767	69
(4) {Gd}100μM	560	77	**(7)** {Gd} 100μM	469	81

4.4. Conclusions

A new nanosized system based on gadolinium for imaging properties and GosAa for anticancer properties was prepared and characterised. SEM and HRTEM analysis showed that nanoparticles present spherical nanometric patterns with intern concentrated areas of Gd compounds. By HRTEM we confirmed one more time the XPS and RES results on Gd tendency to form clusters and to concentrate inside particles as presented in Subchapter 4.2, independently of the synthesis parameter used. GosAa loading capacities were evaluated by surface area and pore volume measurements along with thermogravimetric analysis and showed a higher loading of drug compared to FD2 samples presented in Subchapter 4.2, despite the basic pH used to prepare SiGd-NPs. NMRD profiles revealed that Gd compounds are strongly bonded to silica matrix that behaves like a macromolecule, increasing its relaxivity at high magnetic fields and that GosAa induce increasing of relaxivity. Loading of GosAa into a porous system causes a sustained release mainly characterised by diffusion as proved by the release profile and by the kinetic models results. The sustained release was also evidenced by cytotoxicity studies, cells viability being slight increased for GosAa loaded nanoparticles compared to pure GosAa. T_1 and T_2 weighted images of cellular pellets incubated with nanoparticles showed an appropriate contrast effect for being appropriate candidates for application as magnetic resonance contrast agents. Overall, this study has lead to an *in vitro* safe theranostic compounds that need further research, previous to offer real opportunities for clinical applications.

5. THERANOSTIC LIPOSOMES PREPARED WITH GADOLINIUM COMPOUNDS AND GOSSYPOL ACETIC ACID

5.1. Main objectives

In this study, synthesis and characterisation of theranostic liposomes with dual functions of therapy and diagnosis is presented, by co-encapsulating gossypol acetic acid and gadolinium complex. This design was chosen to have anticancer effects from gossypol acetic acid and MRI contrast sensitivity from gadolinium compound, beside, biocompatibility and low toxicity features offered by liposomes.

5.2. Synthesis and characterization methods

GosAa and Gd complex loaded liposomes were prepared by thin lipid film hydration and polycarbonate membrane extrusion method. The liposomal composition was POPC/CH/DSPE-PEG/GosAa with molar ratio 10:2:0.5:1. For comparison, as control, liposomes without GosAa were also synthesised. For simplicity, the liposomes prepared with GosAa will be further denoted as L-GosAa and the ones without, as L, respectively.

To quantify GosAa, the dialysed liposomes were disrupted with methanol and the lysate absorption was measured at 371 nm. To determine the exact amount of GosAa, a standard calibration curve was used. The Gd concentration and the relaxivity (r_1) of the liposomal formulation was determined by relaxometric procedure using a Spinmaster NMR Relaxometer (Stelar, Mede, Italy) at a Larmor frecquency of 21 MHz by means of the standard inversion recovery pulse sequence.

The stability during storage at 4°C was evaluated in percentage of the remained GosAa and Gd concentration in liposomes, relaxivity (r_1) and particle size over one month.

The stability in biological fluids (plasma) was determined in percentage of the remained encapsulated GosAa, Gd compounds and relaxivity (r_1).

Capabilities of liposomes to be employed also as contrast agents were determined from their NMRD profiles and by a 7 T MRI uptake *in vitro* experiment. Likewise, cytotoxicity studies were performed.

5.3. Results and discussion

As determined by DLS measurements, all the prepared liposomes showed diameter around 100 nm (Table 12). The polydispersity index less than 0.2 indicates a homogenous and monodisperse population. It seems that GosAa presence causes a slight increase in the fluidity of the liposomes walls, fact observed also in other studies [51]. This fact has consequences in size average of the liposomes that showed easiness in extrusion compared

to liposomes without GosAa. Therefore, L-GosAa liposomes are showing slightly decreased sized compared to L liposomes.

Zeta potential indicates high negative values (Table 12), meaning that attraction does not exceed repulsion and the dispersion will be electrically stabilized and will not easily tend to coagulate or flocculate [52]. To note that GosAa salt presence does not significantly change the zeta potential values.

Table 12. DLS measurement results

	Zeta potential (mV)	Size (nm)
L	- 45,3	113
L-GosAa	-46,6	97

In the as prepared liposomes, GosAa and Gd concentration along with the relaxivity values are presented in Table 13. GosAa entrapment efficiency was found to be of 44%, much lower compared to other studies [53]. This is due to special lipids used in present study, POPC being chosen due to its capability to create a more permeable membrane in order to offer access to water molecule to the paramagnetic compounds from inside liposomes [54]. Furthermore, GosAa addition in the liposomes wall induces also changes in relaxivity values. Although L-GosAa encapsulates with 12% more Gd than L, its relaxivity is with 23% higher than L. L-GosAa slightly higher relaxivity could happen because of the smaller size of liposomes prepared in the presence of GosAa, knowing that an inverse relation was observed between liposomes sizes and T_1 relaxivity [55]. On the other part, GosAa interdigitation in the lipid bilayers can also cause an increased permeability of liposomes membrane, with consequences in the relaxivity enhancement.

Table 13. Active compounds concentration and relaxivity of the prepared liposomes

	GosAa concentration {GosAa}(mg/ml)	Gd concentration {Gd} (mM)	r_1 ($s^{-1}mM^{-1}$)
L	0	4.76	4.23
L-GosAa	1.02	5.42	5.55

As shown in Figure 27a and Figure 27b, there were no significant changes in the size or relaxivity values of liposomal formulations suspended in HEPES buffer and stored at 4˚C for 30 days. Nevertheless, some changes could be observed in Gd and GosAa

concentration during storage at 4°C. It is worth mentioning that GosAa has an interesting effect on liposomes behaviour in terms of Gd release, as can be observed in Figure 27c, causing a slower release of Gd complex through membrane pores. GosAa itself also release from liposomes during shelf storage (Figure 27d).

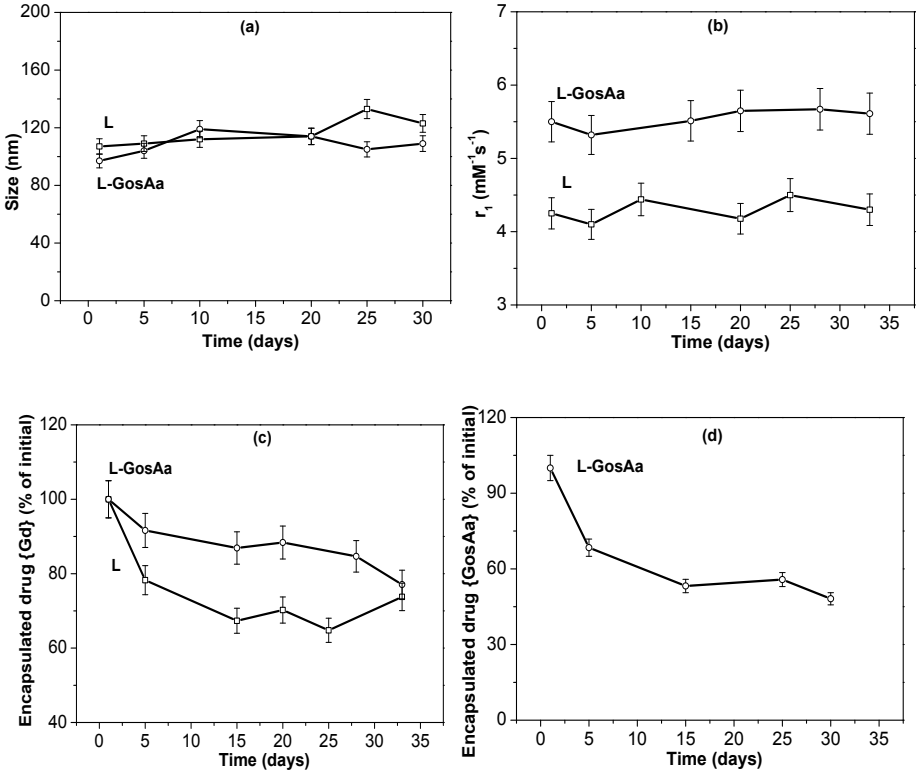

Figure 27. Shelf stability in terms of liposomes size (a), relaxivity (b), Gd concentration {Gd} (c) and GosAa concentration {GosAa} (d) changes

It appears that the reduction of the encapsulated Gd compounds and GosAa concentration in plasma stability experiment occurred faster compared to shelf stability experiment, mainly because of the increased temperature, but also due to FBS medium used (Figure 28). It can be noted that in these conditions of incubation, GosAa presence in the membranes of L-GosAa samples offers some minor protection in terms of Gd release, as it occurs in shelf stability experiment. Although Gd concentration is decreasing, its relaxivity values are remaining almost unchanged during the experiment. Similar but in a more accelerated way, GosAa concentration continuously decreased during 48 h of incubation.

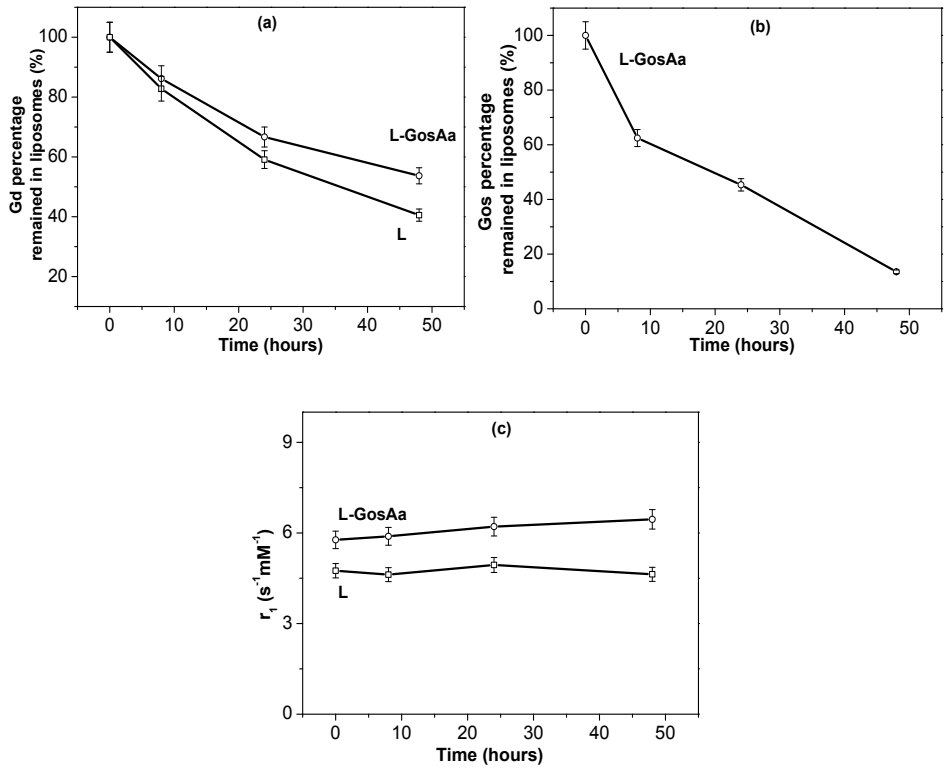

Figure 28. Plasma stability in terms of liposomes Gd concentration {Gd} (a), GosAa concentration {GosAa} (b) and relaxivity (c) changes

We consider these values acceptable, taking into consideration the lipids used in synthesis in order to increase water permeability for a good magnetic resonance response, which has also consequences in Gd compounds and GosAa leakage from inside liposomes. From our point of view, the shelf and plasma stability results were considered appropriate for the liposomal system tested, taking into account the compromise needed to be made to obtain the protons relaxivity effect of Gd compounds and also the therapeutic effect of GosAa. Future studies will seek to find improved solutions.

As can be observed, the shape of NMRD profile of L samples does not significantly differ from the pure gadoteridol NMRD profile (Figure 29) [56]. But GosAa presence in the liposomes walls causes an increase in the relaxivity values and some small changes in the shape of the NMRD profile, especially at high fields. In gadoteridol, Gd ion is coordinated to a macrocyclic compound that reduces its availability as a free ion in order to reduce its adverse effects, knowing that free Gd ion is toxic for the human organism. That is why we can assume reduced interaction between GosAa and Gd, and likewise we can take into consideration the possibility of interaction between GosAa and the macrocyclic part of gadoteridol. GosAa interaction with the macrocyclic part of gadoteridol can cause the formation of a compound with a higher molecular weight. The increase of the

paramagnetic chelate molecular weight and size yields a relaxivity enhancement that is primary due to the restricted rotational mobility of the complex [42] and can be observed in the NMRD profile at higher fields, as a more pronounced band.

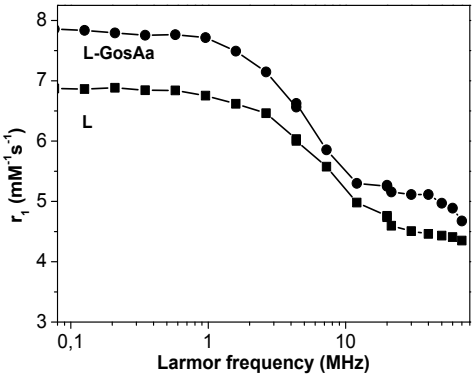

Figure 29. NMRD profiles of the investigated liposomes

The cytotoxicity results (Table 14) show that gadoteridol presence inside liposomes did not dramatically changed the number of viable cells as compared to untreated cells (blank), proving that the Gd complex is safe for cells. GosAa presence inside liposomes walls induces an increased toxicity against TSA cells, thus proving anticancer properties of GosAa. Noteworthy, the same GosAa concentration, not entrapped in liposomes sligtly reduces the number of viable cells compared to GosAa loaded into liposomes, suggesting that the liposomal carrier delivery system could present a minor impact on cells viability.

Table 14. Cytotoxicity studies on TSA breast cancer cells

Samples	Viability (%)	Samples	Viability (%)	Samples	Viability (%)
Blank	100				
L		**L- GosAa**		**GosAa**	
{Gd}10μM	98	{Gd}10μM {GosAa}2.2 μM	94	{GosAa}2.2 μM	90
{Gd}20μM	98	{Gd}20μM {GosAa}4.3 μM	73	{GosAa}4.3 μM	71
{Gd}50μM	96	{Gd}50μM {GosAa}11 μM	60	{GosAa}11 μM	57
{Gd}100μM	95	{Gd}100μM {GosAa}22.8 μM	38	{GosAa}22.8 μM	35

The results of incubation of TSA cells with L and L-GosAa liposomes (Figure 30) showed that gadolinium uptake was proportional to the Gd concentration present in cells growth medium. Small differences were observed between L and L-GosAa samples, at higher concentration of Gd, L-GosAa liposomes being less uptaked by cells compared to L liposomes.

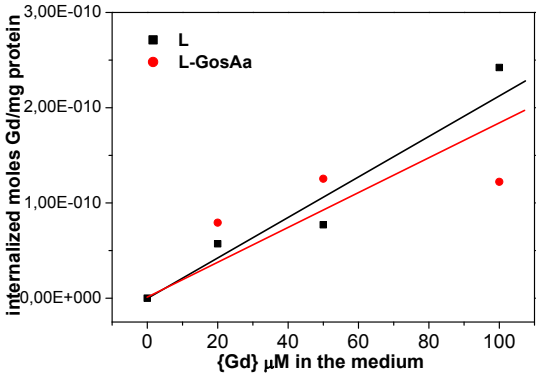

Figure 30. L and L-GosAa (express in Gd moles) uptake in TSA cells after 6 h incubation at 37°. The amount of cell associated Gd has been determined by ICP-MS.

Analysis of MR images (data not shown) obtained from cell pellets at 6 h after incubation showed small signal enhancement compared to control cells. The signal increased proportionally with Gd concentration as it was shown in the uptake experiment and ICP-MS measurements. In this case, enhancement of signal intensity caused by the presence of GosAa in the liposomal system, was confirmed by the T_1 measured values from MRI images, being in good concordance with the results obtained through NMRD profiles (Table 15).

Table 15. T_1 and T_1 decrease percentage values measured at 7 T of pelleted TSA cells

Sample	T_1 (ms)	T_1 decrease (%)	Sample	T_1 (ms)	T_1 decrease (%)
(1) Control cells	2632				
L			**L-GosAa**		
(2) {Gd} 20μM	2421	92	**(5)** {Gd} 20μM	2274	86
(3) {Gd} 50μM	2344	89	**(6)** {Gd} 50μM	2243	85
(4) {Gd} 100μM	2307	88	**(7)** {Gd} 100μM	2127	81

5.4. Conclusions

In this subchapter a new liposomal nanosized system loaded with gadoteridol and GosAa was synthesised and characterised in terms of stability, magnetic resonance properties and cytotoxicity. Liposomes of about 100 nm diameter were synthesised and loaded with a higher quantity of GosAa compared to inorganic carriers presented in Subchapetrs 4.2 and 4.3. Shelf and plasma stability studies showed acceptable behaviour of liposomes at 4°C for a month and at 37°C for 48h, taking into consideration the compromise needed in choosing lipids to have water permeability for contrast agent's

activity and also good loading of GosAa. As it was expected, liposomes showed a better stability at 4°C compared to 37°C. Interestingly, GosAa brings some minor advantages to the liposomal system, by increasing stability of liposomes, through reducing Gd leakage from liposomes. In terms of relaxivity properties, NMRD profiles showed similar features to pure gadoteridol present inside liposomes, but GosAa presence caused an increased relaxivity value and probably a chemical bond between GosAa and gadoteridol, suggested by NMRD profile changing shape. As it was also proved for inorganic SiGd-NPs, GosAa loading into a carrier system like liposomes caused a moderate sustained release into the external medium, proved by the results obtained from cytotoxicity studies. *In vitro* uptake experiments, performed on TSA cells, have demonstrated moderate uptake of the paramagnetic liposomes compared to inorganic carriers discussed in the previous subchapters. T_1 values obtained from MR images highlighted one more time the GosAa effect in increasing relaxivity.

6. GENERAL CONCLUSIONS

Four drug delivery systems were prepared and characterised using different analysis methods.

Firstly, *Gossypium hirsutum* seeds extract was nanoencapsulated in silica microparticles. The drying process influenced both the silica host microparticles and the plant extract. A nanoparticularisation of silica, in H-passivated silica nanoparticles could be observed, through an enhanced fluorescence in pure silica samples. Plant extract entrapment in silica matrix caused an increase in fluorescence signal characteristic to extract. By means of the release profile and kinetic models applied, the system tested presented sustained release characterised mainly by diffusion and the amount released was increased in presence of a higher pH release medium and for freeze dried samples.

Secondly, gossypol was loaded on silica-gadolinium microparticles prepared by sol-gel method at two different pH values. The pH used affected the amount of the loaded gossypol, and its tautomer structure. Acidic pH caused a higher quantity of aldehydic tautomer of gossypol to be loaded on microparticles. Regarding silica-gadolinium structures, it was shown that gadolinium tends to concentrate inside the particles and to form clusters. MRI measurements have shown that samples prepared under acidic conditions especially gossypol loaded silica-gadolinium microparticles caused reduction of relaxation time.

Thirdly, gossypol acetic acid was loaded on silica-gadolinium nanoparticles prepared by sol-gel method with help of surfactants and polymers. These synthesis procedures induced nanometric sizes of silica-gadolinium nanoparticles obtained, with clusters of gadolinium inside. Despite the basic pH used to synthesise these nanoparticles, gossypol acetic acid loading capacities were higher compared to the microparticles prepared under acidic pH conditions, due to enhanced pore volume and surface area along with sonication and repeated loadings applied on the new synthesis process. The relaxivity studies revealed behaviour characteristic to a macromolecule with enhanced relaxivity at higher magnetic fields. One more time, gossypol acetic acid caused an increase in relaxivity of the tested system. The release studies and the kinetic profiles applied showed a sustained release, mainly caused by diffusion. Sustained release of gossypol acetic acid with anticancer effect was proved also by cytotoxicity studies. The *in vitro* uptake studies revealed enhanced cells internalisation of the nanoparticles tested.

Fourthly, gossypol acetic acid was internalised in the walls of gadoteridol loaded liposomes. Liposomes with nanometric sizes and acceptable shelf and plasma stability were obtained. The presence of the lipophilic part in the liposomes caused an enhanced loading of gossypol acetic acid, compared to inorganic systems presented above. The presence of gossypol acetic acid in the liposome's walls offered supplementary stability and improved relaxivity properties. The sustained release character of the liposomal system was proved through cytotoxicity studies. Compared to inorganic carriers presented above, for the liposomal system the *in vitro* uptake experiment showed moderate internalisation into cells.

By this study new structural and behavioural information was brought regarding delivery systems containing lipids, silica, gossypol and gadolinium compounds in order to be used as sustained and/or theranostic compounds. Further studies are necessary to improve even more the tested systems. As a start idea, a new silica-liposome hybrid system could be taken into consideration to obtain by this way the benefits to upload high amounts of drug from liposomes and the benefits of stability and relaxivity properties from silica-gadolinium nanoparticles.

SELECTED BIBLIOGRAPHY

[1] P.U. Rani, S. Pratyusha. Defensive role of *Gossypium hirsutum L*. anti-oxidative enzymes and phenolic acids in response to *Spodoptera litura F*. feeding. J Asia Pac Entomol 2013;16:131-6.

[2] L. Yildiz-Aktas, S. Dagnon, A. Gurel, E. Gesheva, A. Edreva. Drought tolerance in cotton: Involvement of non-enzymaticros-scavenging compounds. J Agron Crop Sci 2009;195:247-53.

[3] K.E. Lege, J.T. Cothren, C.W. Smith. Phenolic acid and condensed tannin concentrations of six cotton genotypes. Environ Exp Bot 1995;35:241-9.

[4] A. Hashimoto, T. Kameoka. Applications of Infrared spectroscopy to biochemical, food, and agricultural processes. Applied Spectroscopy Reviews 2008;43:416-51.

[5] Y. Li, S. Sun, Q. Zhou, Z. Qin, J. Tao, J. Wang, X. Fang. Identification of American ginseng from different region using FT-IR and two-dimensional correlation IR spectroscopy. Vib Spectrosc 2004;36:227-32.

[6] H. Schultz, M. Baranska. Identification and quantification of valuable substances by IR and Raman spectroscopy. . Vib Spectrosc 2007;43:13-25.

[7] S. Zavoi, F. Fetea, F. Ranga, R.M. Pop, A. Baciu, C. Socaciu. Comparative fingerprint and extraction yield of medicinal herbphenolics with hepatoprotective potential, as determined by UV-Vis and FT-MIR spectroscopy Not Bot Horti Agrobo 2011;39:82-9.

[8] L. Qiao, Y. Sun, R. Chen,Y. Fu, W. Zhang, X. Li, J. Chen, Y. Shen, X. Ye. Sonochemical effects on 14 flavonoids common in citrus: Relation to stability. Plos One 2014;9:e87766.

[9] W.J. Sandberg, M. Låg, J.A. Holme, B. Friede, M. Gualtieri, M. Kruszewski, P.E. Schwarze, T. Skuland, M. Refsnes. Comparison of non-crystalline silica nanoparticles in IL-1β release from macrophages. Part Fibre Toxicol 2012;9:1-13.

[10] D. Quintanar-Guerrero, A. Ganem-Quintanar, M.G. Nava-Arzaluz, E. Piñón-Segundo. Silica xerogels as pharmaceutical drug carriers. Expert Opin Drug Del 2009;6:485-98.

[11] C. Pinto Reis, R.J. Neufeld, A.J. Ribeiro, F. Veiga. Nanoencapsulation I. Methods for preparation of drug-loaded polymeric nanoparticles. Nanomed-Nanotechnol 2006;2:8-21.

[12] S. Ek, A. Root, M. Peussa, L. Niinisto. Determination of the hydroxyl group content in silica by thermogravimetry and a comparison with 1 H MAS NMR results. Thermochim Acta 2001;379:201-12.

[13] I. Lacatusu, N. Badea, D. Bojin, S. Iosub, A. Meghea. Novel fluorescence nanostructured materials obtained by entrapment of an ornamental bush extract in hybrid silica glass. J Sol-Gel SciTechn 2009;51:84-91.

[14] G.R. Gamble, J.A. Foulk. Quantitative analysis of cotton (*Gossypium hirsutum*) lint trash by fluorescence spectroscopy. J Agr Food Chem 2007;55:4940-3.

[15] D.A. Eckhoff, J.D.B. Sutin, R.M. Clegg, E. Gratton, E.V. Rogozhina, P.V. Braun. Optical characterization of ultrasmall Si nanoparticles prepared through electrochemical dispersion of bulk Si. J Phys Chem B 2005;109:19786-97.

[16] J.R. Lakowicz. Quenching of fluorescence. In: Lakowicz J, editor. Principles of fluorescence spectroscopy: Springer US; 2006. p. 277-330.

[17] D. Teoli, L. Parisi, N. Realdon, M. Guglielmi, A. Rosato, M. Morpurgo. Wet sol–gel derived silica for controlled release of proteins. J Control Release 2006;116:295-303.

[18] Z. Wu, H. Joo, I.S. Ahn, J.H. Kim, C.K. Kim, K. Lee Design of doped hybrid xerogels for a controlled release of brilliant blue FCF. J Non-Cryst Solids 2004;342:46-53.

[19] E. Verraedt, M. Pendela, E. Adams, J. Hoogmartens, J.A. Martens Controlled release of chlorhexidine from amorphous microporous silica. J Control Release 2010;142:47-52.

[20] S. R. Veith, E. Hughes, S.E. Pratsinis. Restricted diffusion and release of aroma molecules from sol-gel-made porous silica particles. J Control Release 2004;99:315-27.

[21] R.H. Muller, C. Jacobs, O. Kayser. Nanosuspensions as particulate drug formulations in therapy Rationale for development and what we can expect for the future. Advanced drug delivery reviews 2001;47:3-19.

[22] L.C. Weiss, D.P. Thibodeaux. Electrodynamic method for separating components. Google Patents; 1985.
[23] J. Reyes, J. Allen, N. Tanphaichitr, A. R. Bellve, D. J. Benos Molecular mechanisms of gossypol action on lipid membranes. The Journal of biological chemistry 1984;259:9607-15.
[24] M.S. Kuk, R. Tetlow Gossypol removal by adsorption from cottonseed miscella. Journal of the American Oil Chemists Society 2005;82:905-9.
[25] K.N. Campbell, R.C. Morris, R. Adams. The structure of gossypol. I. Journal of the American Chemical Society 1937;59:1723-8.
[26] Y.L. Shen, S.H. Yang, L.M. Wu, X.Y. Ma. Study on structure and characterization of inclusion complex of gossypol/beta cyclodextrin. Spectrochimica Acta Part A-Molecular Spectroscopy 2005;61:1025-8.
[27] B. Brzezinski, J. Olejnik, S. Paszyc. Fourier transform infrared study on the identification of gossypol tautomers. Journal of Molecular Structure 1990;239:23-31.
[28] M.E.S. Mirghani, Y.B. Che Man. A new method for determining gossypol in cottonseed oil by FTIR spectroscopy. Journal of the American Oil Chemists Society 2003;80:625-8.
[29] B. Brzezinski, B. Marciniak, S. Paszyc, G. Zundel. The tautomerization of gossypol as a function of the presence of Ni^{2+}, Cu^{2+} or Zn^{2+} cations. Journal of Molecular Structure 1992;268:61-6.
[30] B. Brzezinski, S. Paszyc, G. Zundel. The structure of Gossypol as a function of the presence of HAuCl, and of Be^{2+} ions. Journal of Molecular Structure 1991;246:45-51.
[31] P. Przybylski, G. Bejcar, W. Schilf, B. Kamienski, B. Brzezinski. ^{13}C, ^{15}N CP-MAS as well as FT-IR studies of gossypol derivatives with aromatic substituents in solid. Journal of Molecular Structure 2007;826:150-5.
[32] N.S. Ilkevycha, G. Schroeder, V.I. Rybachenko, K.Y. Chotiy, R.A. Makarova. Vibrational spectra, structure and antioxidant activity of gossypol imine derivatives. Spectrochimica Acta Part A 2012;86:328-35.
[33] S. Simon, I. Ardelean, S. Filip, I. Bratu, I. Cosma. Structure and magnetic properties of Bi_2O_3–GeO_2–Gd_2O_3 glasses. Solid State Communications 2000;116:83-6.
[34] K. Sinkó. Influence of chemical conditions on the nanoporous structure of silicate aerogels. Materials 2010;3:704-40.
[35] S. Simon, R.V.F. Turcu, T. Radu, M. Moldovan, V. Simon. Multispectroscopic investigation of silanised glass particles for dental fillers. Journal of Optoelectronics and Advanced Materials 2009;11:1660-70.
[36] O. Ponta, C. Gruian, E. Vanea, B. Oprea, H.J. Steinhoff, S. Simon. Nanostructured biomaterials/biofluids interface processes: titanium effect on methaemoglobin adsorption on titanosilicate microspheres. Journal of Molecular Structure 2013;1044:2-9.
[37] C.A. Milea, C. Bogatu, A. Duţă. The influence of parameters in silica sol-gel process. Bulletin of the Transilvania University of Braşov 2011;4:59-66.
[38] A. Puri, K. Loomis, B. Smith, J.H. Lee, A. Yavlovich, E. Heldman, R. Blumenthal. Lipid-based nanoparticles as pharmaceutical drug carriers: from concepts to clinic. Critical Reviews In Therapeutic Drug Carrier Systems 2009;26:523-80.
[39] Z. Wang, B. Chen, G. Quan, F. Li, Q. Wu, L Dian, Y. Dong, G. Li, C. Wu. Increasing the oral bioavailability of poorly water-soluble carbamazepine using immediate-release pellets supported on SBA-15 mesoporous silica. International journal of nanomedicine 2012;7:5807-18.
[40] D. Halamová, M. Badanicová, V. Zelenák, T. Gondová, U. Vainioc. Naproxen drug delivery using periodic mesoporous silica SBA-15. Applied Surface Science 2010;256:6489-94.
[41] M.A. Ballem, F. Söderlind, P. Nordblad, P.-O. Käll, M. Odéna. Growth of Gd_2O_3 nanoparticles inside mesoporous silica frameworks. Microporous And Mesoporous Materials 2013;168:221-4.
[42] S. Aime, D. Delli Castelli, S. Geninatti Crich, E. Gianolio, E. Terreno. Pushing the sensitivity envelope of lanthanide-based magnetic resonance imaging (mri) contrast agents for molecular imaging applications. Accounts of Chemical Research 2009;42:822-31.
[43] S. Aime, M. Botta, M. Fasano, E. Terreno. Lanthanide(III) chelates for NMR biomedical applications. Chemical Society reviews 1998;27:19-29.

[44] Y. Shao, X.Tian, W. Hu, Y. Zhang, H. Liu, H. He, Y. Shen, F. Xie, L. Li. The properties of Gd_2O_3-assembled silica nanocomposite targeted nanoprobes and their application in MRI. Biomaterials 2012;33:6438-46.
[45] C.R. Kim, J.S. Baeck, Y. Chang, J.E. Bae, K.S. Chaecd, G.H. Lee. Ligand-size dependent water proton relaxivities in ultrasmall gadolinium oxide nanoparticles and in vivo T1 MR images in a 1.5 T MR field. Physical Chemistry Chemical Physics 2014;16:19866-73.
[46] C. V. Moraru, E. Vanea, K. Magyari, M. Tamasan, A. S. Farcasanu, F. Loghin, S. Simon. Silica-gadolinium particles loaded with gossypol for simultaneous therapeutic effect and MRI contrast enhancement. J Sol-Gel Sci Techn 2014;72:593-601.
[47] S. Dumas, V. Jacques, W.C. Sun, J. S. Troughton, J. T. Welch, J. M. Chasse, H. Schmitt-Willich, P. Caravan. High relaxivity MRI contrast agents part 1: Impact of single donor atom substitution on relaxivity of serum albumin-bound gadolinium complexes. Investigative Radiology 2010;45:600-12.
[48] V. Jacques, S. Dumas, W.C. Sun, J.S. Troughton, M.T. Greenfield, P. Caravan. High relaxivity MRI contrast agents part 2: Optimization of innerand second-sphere relaxivity. Investigative Radiology 2010;45:613-24.
[49] S. Dash, P. Narasimha Murthy, P. Chowdhury. Kinetic modeling on drug release from controlled drug delivery systems. Acta Poloniae Pharmaceutica 2010;67:217-23.
[50] S. Ullah Shah, K. Ullah Shah, A. Rehman, G.M. Khan. Investigating the in vitro drug release kinetics from controlled release diclofenac potassium-ethocel matrix tablets and the influence of co-excipients on drug release patterns. Pak J Pharm Sci 2011;24:183-92.
[51] M. Ionov, I. Tukfatullina, B. Salakhutdinov, N. Baram, M. Bryszewska, T. Aripov. The interaction of PVP complexes of gossypol and its derivatives with an artificial membrane lipid matrix. Cellular and Molecular Biology Letters 2010;15:98-117.
[52] B. Heurtault, P. Saulnier, B. Pech, J. E. Proust, J.P. Benoit. Physico-chemical stability of colloidal lipid particles. Biomaterials 2003;24:4283–300.
[53] G. Zhai, J. Wu, X. Zhao, B. Yu, H. Li, Y. Lu, W. Ye, Y.C. Lin, R.J. Lee. A liposomal delivery vehicle for the anticancer agent gossypol. Anticancer Research 2008;28:2801-6.
[54] E. Terreno, A. Sanino, C. Carrera, D. Delli Castelli, G. B. Giovenzana, A. Lombardi, R. Mazzon, L. Milone, M. Visigalli, S. Aime Determination of water permeability of paramagnetic liposomes of interest in MRI field. Journal of Inorganic Biochemistry 2008;102:1112-9.
[55] K. Ghaghada, C. Hawley, K. Kawaji, A. Annapragada, S. Mukundan T1 relaxivity of core-encapsulated gadolinium liposomal contrast agents—effect of liposome size and internal gadolinium concentration. Academic Radiology 2008;15:1259–63.
[56] M. Filippi, J. Martinelli, G. Mulas, M. Ferraretto, E. Teirlinck, M. Botta, L. Tei, E. Terreno. Dendrimersomes: a new vesicular nano-platform for MR-molecular imaging applications. Chemical Communications 2014;50:3453-6.

APPENDIX

ISI published papers

1. C.V. Moraru, E. Vanea, K. Magyari, M. Tamasan, A. S. Farcasanu, F. Loghin, S. Simon. Silica-gadolinium particles loaded with gossypol for simultaneous therapeutic effect and MRI contrast enhancement. J Sol-Gel Sci Technol, 2014, 72, (3), 593-601.

2. E. Vanea, **C. Moraru**, A. Vulpoi, S. Cavalu, V. Simon. Freeze dried and spray-dried zinc-containing silica microparticles entrapping insulin. Journal of Biomaterials Applications, 2014, 28, (8), 1190-1199.

BDI published papers

1. E. Vanea, **C. Moraru**, S. Muresan, R. Moldovan, A. Filip, A. Muresan, S. Simon. High field MRI investigation of eye structures after UV-B irradiation. Studia UBB Physica, 2013, 58, (LVIII), 2, 67-74.

2. E. Vanea, C. Gruian, L. Pătcaş, **C. V. Moraru**, V. Simon. Preliminary study regarding the biocompatibility of some new biomaterials designed for synergic hyperthermia/radiotherapy applications. Studia UBB Physica, 2013, 58, (LVIII), 1, 67-76.

Submitted paper

1. **C.V. Moraru**, K. Magyari, M. Tamasan, S. Suarasan, D. Muntean, L. Vlase, F. Loghin, S. Simon. Synthesis and characterisation of *Gossypium hirsutum* seeds extract nanoencapsulated in silica microparticles. Journal of Controlled Release

Participation to conferences

1. A. Berar, A. Kui, **C. Moraru**, A. Farcasanu, F. Turcu, L. Lascu, S. Simon, R. S. Campian. Imaging and histopatological evaluation of induced experimentally periapical lesions in rats. University of Medicine and Pharmacy days "Iuliu Haţieganu" Cluj-Napoca, Romania, 2.12-5.12, 2014

2. C.V. Moraru, E. Vanea, M. Tamasan, K. Magyari, A. S. Farcasanu ,F. Loghin, S. Simon. Multi functional silica-gadolinium particles loaded with gossypol for theranostic application. Advanced Spectroscopies on Biomedical and Nanostructured Systems, Cluj-Napoca, Romania, 7.09-10.09, 2014.

3. C.V. Moraru, E. Vanea, C. Gruian, M. Tamasan, K. Magyari, O. Ponta, A. Vulpoi, F. Loghin, S. Simon. Bovine serum albumin functionalized silica-gadolinium nanoparticles embedded with gossypol as theranostic compounds. ESCDD - 13th European Symposium on Controlled Drug Delivery, Egmond aan Zee, Holland, 16.04-18.04, 2014.

4. E. Vanea, C. Gruian, L. Pătcaş, **C.V. Moraru**, V. Simon. EPR investigation of protein adsorption onto biomaterials designed for dual hyperthermia/radiotherapy applications. Bioceramics 25, 25th Symposium and Annual Meeting of International Society for Ceramics in Medicine. Bucuresti, Romania. 07.11-10.11, 2013.

5. C.V. Moraru, S. Suarăsan, E. Vanea, S. Simon. Structural analysis of silica and silica-gadolinium xerogels loaded with *Gossypium hirsutum* seeds extract. Bioceramics 25, 25th Symposium and Annual Meeting of International Society for Ceramics in Medicine. Bucuresti, Romania. 07.11-10.11, 2013.

6. E. Vanea, **C. Morar**, S. Cavalu, V. Simon. Insulin Entrapment and release from zinc-containing silica microparticles. 3rd Termis world congress. Wien, Austria 05.09.08.09, 2012.

7. C.V. Moraru, E. Vanea, F. Loghin, S. Simon. Structural analysis of gossypol loaded silica-gadolinium particles intended for cancer treatment. 5th International Conference Biomaterials, Tissue Engineering & Medical Devices. Constanța, Romania 24.08-01.09, 2012.

ACKNOWLEDGEMENTS

The laboratory work for this thesis was carried out mainly at Institute of Interdisciplinary Research in Bio-Nano-Sciences and National Centre of Magnetic Resonance from Babeş-Bolyai University, Cluj-Napoca, but also at Molecular Biotechnology Centre, Turin University, Turin, Italy and Department of Pharmaceutical Technology and Biopharmaceutics, Faculty of Pharmacy, Cluj-Napoca.

I would like to express my sincere gratitude to my advisors, Prof. Dr. Simion Simon and Prof. Dr. Felicia Loghin for their guidance, understanding, consideration and support throughout the course of this research. I would like to extend my gratitude to Prof. Dr. Todica Mihai, Conf. Dr. Lucian Baia, and Conf. Dr. Raluca Ciceo-Lucăcel, for serving on my Ph.D. guidance committee as well as providing invaluable instructions and recommendations.

Also, I would like to thank my past and current group members from Institute of Interdisciplinary Research in Bio-Nano-Sciences for helping me with measurements and results interpretation.

I would like also to thank members in the National Centre of Magnetic Resonance from Babeş-Bolyai University, Cluj-Napoca for their help and valuable advices.

I am grateful to Prof. Dr. Silvio Aime for giving me the opportunity to work with the research group from Molecular Biotechnology Centre in Turin. My special thanks to all Centre'members for all the discussions and help I received, especially to Dr. Eliana Gianolio for her interests and supports of this work.

Special appreciation is extended to Prof. Dr. Sorin Leucuța, Prof. Dr. Marcela Achim and Prof. Dr. Laurean Vlase from Department of Pharmaceutical Technology and Biopharmaceutics, Faculty of Pharmacy, Cluj-Napoca for the advices, measurements and substances offered for this research.

Great appreciation to Prof. Dr. Daniela Popa for valuable discussion on my research and to Prof. Dr. Arno Gutleb for *in vitro* studies performed in Luxembourg at Public Research Centre "Gabriel Lippmann", Environment and Agro-Biotechnologies Department.

I want to warmly thank Prof. Dr. Simona Mirel for the opportunity to work with her and for all the support offered.

This work was possible due to the financial support of the Sectorial Operational Program for Human Resources Development 2007-2013, co-financed by the European Social Fund, under the project number POSDRU/159/1.5/S/132400 with the title „Young successful researchers – professional development in an international and interdisciplinary environment" and to BIOMAPIN PCCE-101/2008 project granted by the Romanian National University Research Council.

Finally, I am deeply grateful to my parents, my sister and especially my husband, for fully supporting me in all aspects during these years.